



Applications of Generative Adversarial Networks (GANs) in Positron Emission Tomography (PET) imaging: A review

Ioannis D. Apostolopoulos¹ · Nikolaos D. Papathanasiou² · Dimitris J. Apostolopoulos² · George S. Panayiotakis¹

Received: 22 November 2021 / Accepted: 12 April 2022

© The Author(s), under exclusive licence to Springer-Verlag GmbH Germany, part of Springer Nature 2022

Abstract

Purpose This paper reviews recent applications of Generative Adversarial Networks (GANs) in Positron Emission Tomography (PET) imaging. Recent advances in Deep Learning (DL) and GANs catalysed the research of their applications in medical imaging modalities. As a result, several unique GAN topologies have emerged and been assessed in an experimental environment over the last two years.

Methods The present work extensively describes GAN architectures and their applications in PET imaging. The identification of relevant publications was performed via approved publication indexing websites and repositories. Web of Science, Scopus, and Google Scholar were the major sources of information.

Results The research identified a hundred articles that address PET imaging applications such as attenuation correction, de-noising, scatter correction, removal of artefacts, image fusion, high-dose image estimation, super-resolution, segmentation, and cross-modality synthesis. These applications are presented and accompanied by the corresponding research works.

Conclusion GANs are rapidly employed in PET imaging tasks. However, specific limitations must be eliminated to reach their full potential and gain the medical community's trust in everyday clinical practice.

Keywords Generative Adversarial Networks · Positron Emission Tomography · Nuclear Medicine · Deep Learning

Introduction

Generative Adversarial Networks (GAN) are a dominant image generation strategy with countless applications. GANs dedicated to imaging tasks are special topologies of Convolutional Neural Networks (CNN), often addressed as Deep Learning (DL), though DL has a broader meaning. CNNs are special Neural Networks (NN) that expertise mainly in images. The mathematical operation of convolution is the cornerstone of CNNs, which transform the input data to feature maps, representing the input data on a higher and more abstract level. Typical GANs consist of two CNNs,

namely a generator and a discriminator. The generator CNN outputs a synthetic image, given a latent vector as input. The discriminator is responsible for distinguishing between authentic and synthetic images. Meanwhile, a specific loss function calculates the back-propagated losses to the generator. The two CNNs play a minimax game until the generator has learned how to deceive the discriminator and vice-versa.

Before GANs had emerged, the synthetic images were produced by applying geometrical, texture, histogram and other transformations. As a result, the synthetic images lacked diversity and limited their utilisation. GANs are employed in a broad range of domains, including image-to-image translation, text-to-image translation, face frontal-view generation, photograph editing, super-resolution, 3D object generation, even cybersecurity [1]. Their applications in several sectors of human activity are described in full detail [2].

Medical imaging is a challenging field of application for GANs. Medical information is a disparate source of information. Although performed by algorithms and methods that share the same fundamental concepts as conventional image-processing algorithms, medical

This article is part of the Topical Collection on Advanced Image Analyses (Radiomics and Artificial Intelligence).

✉ Ioannis D. Apostolopoulos
ece7216@upnet.gr

¹ Department of Medical Physics, School of Medicine, University of Patras, Patras, Greece

² Laboratory of Nuclear Medicine, University Hospital of Patras, Rio, Greece

image processing poses critical challenges. Medical images capture sensitive information, and their diagnostic interpretation affects clinical decisions. Hence, medical imaging concepts, methods, and computational models must be accountable. GANs have rapidly found application in this domain and enjoy research attention by companies, institutes and researchers.

Nuclear Medicine (NM) imaging differs from other imaging modalities due to applying radioactive tracers injected into the human body before image acquisition by specific detectors. As a result, NM imaging is a challenging field for Artificial Intelligence (AI) methods, specifically DL and GANs. Nensa et al. [3] gave a short review of AI applications in NM, separating the domains of interest into planning, scanning, reading, and reporting. They also reported a brief timeline of major AI developments over the last 80 years. A short review of AI and ML in NM is presented in [4, 5].

In Koshino et al. [6], the authors reviewed several GAN-based topologies with medical and molecular imaging applications. Modality conversion, image de-noising, image reconstruction, domain adaptation, and super-resolution were mainly described for CT and MRI imaging.

Cheng et al. [7] presented the applications of AI in NM. Their review was focused on scatter correction, image reconstruction, multiple modality image fusion, and internal dosimetry. Radiation exposure reduction and artefact correction in medical imaging using GANs were reviewed in [8]. Arabi et al. [9] extensively reviewed AI methods in PET and SPECT imaging. Although they examined multiple application domains, the representation of GANs was sparse (8 scientific papers). Manjooran et al. [10] presented AI methods for cross-modality synthesis from MRI to PET, including selected GANs. Zaharchuk [11] examined DL applications for hybrid PET/MR and PET/CT imaging, including low-count PET imaging and image synthesis. The same author reviewed AI methods for the same modalities to address challenges such as attenuation correction, PET reconstruction, dose minimisation, fast-scanning, and cross-modality synthesis [12]. In the review paper of [13], the authors described the applications of Machine Learning and DL methods in quantitative PET. More specifically, they focused on the low-count PET image reconstruction method and PET image attenuation correction.

Recent literature research has not systematically represented GAN's applications and challenges in PET imaging. In the present review article, the reader can get a coherent and comprehensive insight on the GAN topologies and implementations that facilitate PET imaging activities. Research has been performed to identify and distinguish 100 related publications. The selection criteria, the research keywords, and methods are presented and discussed.

Materials and Methods

Literature methodology and criteria

The identification of relevant publications was performed via approved publication-indexing websites and repositories. Web of Science, Scopus, and Google Scholar were the major sources of information. Multiple keyword combinations were used to mine research papers and select the initial library, including: "Generative Adversarial Networks", "GAN(s)", "Deep Learning", and "Positron Emission Tomography-PET". The survey covered publications from January 2015 till November of 2021. During this period, a total number of 1986 publications qualified to constitute the initial library.

The publications were scanned to detect the keywords of interest in their main texts and exclude irrelevant publications. Initially, 121 publications were qualified for review. There were 11 review papers, most of which were appropriately referenced in the present article. Subsequently, 100 publications refer to applications of GANs in PET imaging.

Only English-language publications or an extensive English abstract were considered in the particular survey. Unpublished preprints were included but not extensively discussed due to the absence of peer review when this survey was conducted. The complete process is provided in Fig. 1

Generative Adversarial Networks: a special network topology

GANs belong to the so-called generative modelling. Generative modelling is an unsupervised learning procedure in ML that reveals patterns and contextual features in the input data to generate new samples belonging to the original training dataset given their similarity. GANs are unique Neural Network-based topologies [14]. Typical GANs in image synthesis tasks are called Deep Convolutional GANs (DC-GANs) and consist of two independent CNNs, as shown in Fig. 2. Those two CNNs are trained simultaneously and are responsible for different tasks. The first CNN is the generator responsible for synthesising new images; the second network is the discriminator, distinguishing between synthetic and authentic images. The two networks play a minimax game. The discriminator becomes better at distinguishing between fake and real images during the training process, and the generator improves by producing authentic-like images. The two networks communicate with each other through an objective function. The generator learns to update its parameters

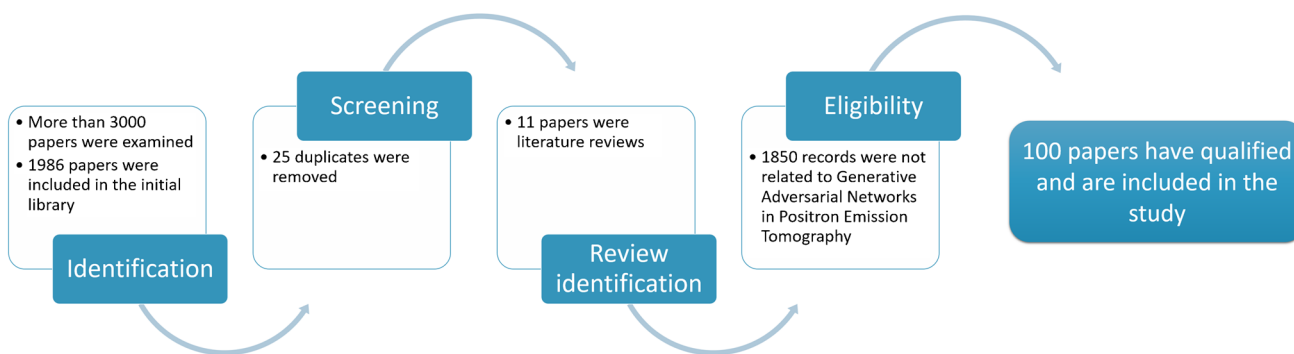
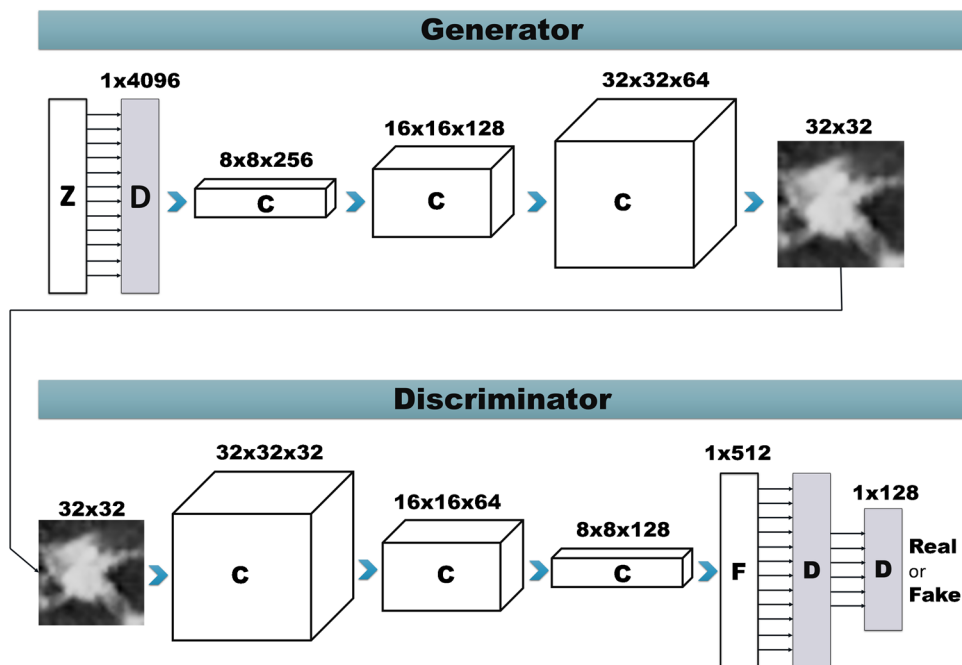


Fig. 1 Literature review process

Fig. 2 Example of a GAN topology. A 32 × 32 synthetic image is produced from the generator, which gradually up-samples a latent space (Z) connected to a dense layer (D) to the output image using 256, 128, and 64 convolution (C) filters. The discriminator processes either a realistic or a synthetic image by applying several convolutions to extract important features. Those features are flattened (F) before a densely connected network (D) decides if the input image is real or fake



during each iteration to deceive the discriminator. Ideally, the optimal point would be when the discriminator fails to recognise the synthetic images. At that point, the generator is no longer becoming better. Conversely, when the generator fails to synthesise authentic-like images, the discriminator is no longer improving. Based on the robustness of those two networks and the quality and quantity of the training data, the generated examples can plausibly be considered real by the human eye.

Fundamentals of GANs

The first network acts as an image generator, named Generator (G). The second network's purpose is to distinguish between synthetic and authentic images, referred to as Discriminator (D). The generator's input is an arbitrary latent space, symbolised as z . The output of G is a synthetic image,

symbolised as X_g . Apart from the synthetic (fake) image X_g , the discriminator's input is also an actual image, X_r . The output of D is an assigned probability of the image being fake or real [14].

The G output is an image, x_g , expected to visually resemble the actual sample x_r , selected from the real data distribution $p_r(x)$. The nonlinear mapping function learned by G parametrised by θ_g is denoted as $x_g = G(z; \theta_g)$. The discriminator's input is either a real or a generated image. The output of the D, y_1 , is a single value indicating the probability of the input being real or fake. The mapping learned by D parametrised by θ_d is denoted as $y_1 = D(x; \theta_d)$.

A distribution $p_g(x)$ is formed by the generated samples. After successful training, this distribution is expected to approximate $pr(x)$. Although G is trained to confuse D as much as possible after a specific number of iterations, D and G desire to become experts in their tasks.

Practically, as D improves its efficiency in distinguishing fakes from real images, G becomes better at generating fake images, which are difficult to distinguish from the real.

The gradient information is back-propagated from D to G, so G adapts its parameters to produce an output image that D cannot detect at the next step. The training objectives of D and G are mathematically formulated into the following equations:

$$L_D^{GAN} = \max E_{x_r \sim p_r(x)} [\log D(x_r)] + E_{x_g \sim p_g(x)} [\log(1 - D(x_g))]$$

$$L_G^{GAN} = \min E_{x_g \sim p_g(x)} [\log(1 - D(x_g))]$$

Mathematically, D is simply a binary classifier with a maximum log-likelihood objective. If the discriminator D is trained to optimality before the next generator G updates, then minimising L_G^{GAN} is proved to be equivalent to minimising the Jensen–Shannon (JS) divergence between $p_r(x)$ and $p_g(x)$ [5]. After training, the desired outcome is that the samples x_g , produced by G, should approximate the real data distribution $p_r(x)$.

The above mathematical process reveals the context of the minimax game, which refers to the simultaneous optimisation of the two CNN components. More specifically, “min” refers to minimising the generator’s loss and “max” maximising the discriminator’s loss. The discriminator maximises the average log probability of authentic images and the log of the inverse probability for synthetic images. At the same time, the generator attempts to minimise the log of the inverse probability, as predicted by the discriminator for the synthetic images.

Plenty of GAN topologies have been proposed. The most utilised are summarised in the following sub-sections. The reader can inspect their architecture variations in Fig. 3. Also, in Fig. 11, the topologies are sorted based on their utilisation frequency.

Conditional GAN (cGAN)

The standard baseline, occasionally called Vanilla GAN, is not designed to handle image synthesis following specific user-defined conditions. Conditional GANs [15] are

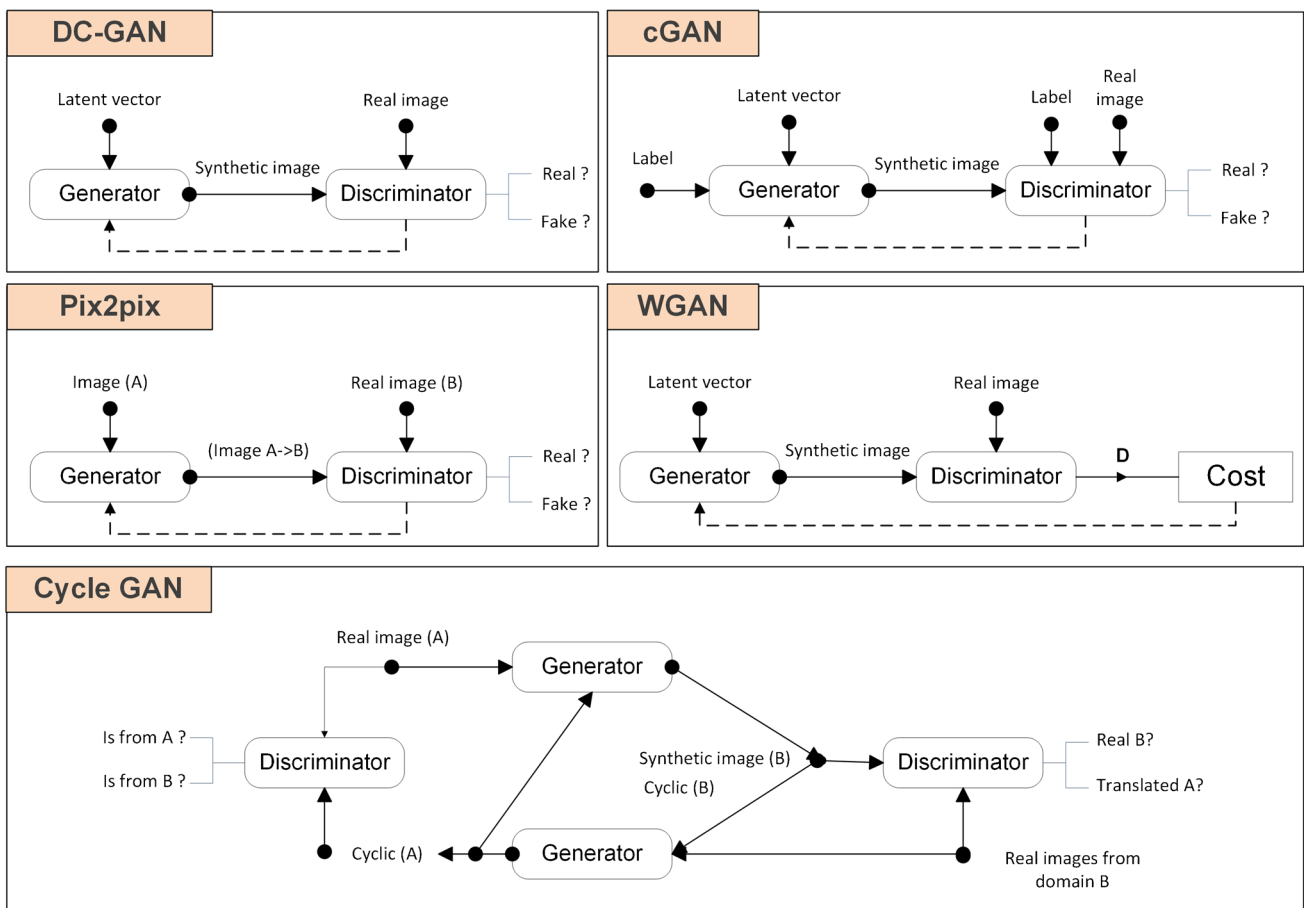


Fig. 3 Main GAN topologies employed in PET imaging

networks aiming to generate a synthetic image characterised by a specific set of predefined features. For example, the desired synthetic image may vary in terms of the area of interest, the modality, or class. As an example, a cGAN may be developed to generate benign-only pulmonary nodules, given a training set of both benign and malignant samples. cGANs achieve this because their generators can receive an auxiliary input label. cGANs can generally synthesise images and capture knowledge that discriminates the images according to their conditional labels.

Pix2Pix

Pix2pix [16] is an image-to-image translation GAN. Pix2pix learns by pairwise training sets. Such networks receive real image pairs and pairs of real and synthetic samples. Hence, they learn relationships that translate one image to the other. The above is particularly useful in situations where medical staff are interested in a cross-modality examination, wherein some images are missing, but their translations exist. Pix2pix uses a different loss function than the cGAN, which ensures that the generated image could belong to the content of the target domain and could also be a translation of the input image. The loss that the generator tries to minimise is twofold in this case. The generator of Pix2pix is a U-Net type encoder–decoder network, which does not receive its input from the latent space as it happens in the baseline GAN. Instead, its input is an image from the source domain. This is why conventional CNNs could not serve as generators, and encoder–decoder networks are used instead. The input images are progressively down-sampled and up-sampled to produce the output image during this process.

CycleGAN

CycleGAN [17] consists of two generators and two discriminators. The generators convert an image of a given domain into another domain, while the discriminators determine whether an image that belongs to a given domain is synthesised by images of the same domain or from another. Similar to Pix2pix, CycleGAN is mainly used for image-to-image translation and is widely accepted because it does not need a large amount of pair data to operate.

In CycleGAN, the inputs images of the first generator belong to the first domain, and the output images are expected to belong to the second domain. Conversely, the second generator receives images from the second domain and generates images that could be plausible in the first domain. The CycleGAN architecture includes

cycle consistency, a novel component compared to conventional GANs. Cycle consistency refers to the approach wherein the output of the first generator is also used as input to the second generator, whilst the output of the second generator should be identical to the original image and vice-versa. This ensures that an image of the first domain can be effectively translated to an image of the second domain. Furthermore, the translated image can be translated back to the original by the second generator. Cycle consistency introduces an additional loss that measures the difference between the generated output of the second generator and the original image and the reverse.

Wasserstein GAN (WGAN)

WGAN [18] is a GAN extension that implements alternative ways of training the generator network to precisely approximate the distribution of the observed data. In WGAN, the discriminator is substituted by a critic that scores the realness of the synthetic image. In addition, this GAN utilises the Wasserstein distance as a similarity measure for comparisons between synthetic and authentic data. Subsequently, WGAN uses a different loss function, which derives from the Wasserstein Distance. Empirical implementations have shown that WGAN may be suitable for synthesising better-detailed images. WGAN is also more robust and stable GAN than the baseline models, as the parameter tuning and the network architecture play a less important role in the network's stability and avoid model collapse—a very common setback of GANs.

Results

Metrics

This review identified 100 publications since 2017. There was an exponential growth in the total number of relevant publications since 2017, highlighting the growing interest in the applications of GANs in PET imaging.

Nine (9) domains of GAN applications in PET imaging were identified (Fig. 4), namely cross-modality synthesis (26 publications), full-count PET estimation (from low-dose, fast scan, or sampling reduction) (22 publications), attenuation correction (20 publications), data augmentation and disease classification (11 publications), PET quantification (6 publications), de-noising, artefact removal, motion and scatter correction (5 publications), segmentation (4 publications), image fusion (4 publications), and super-resolution (2 publications).

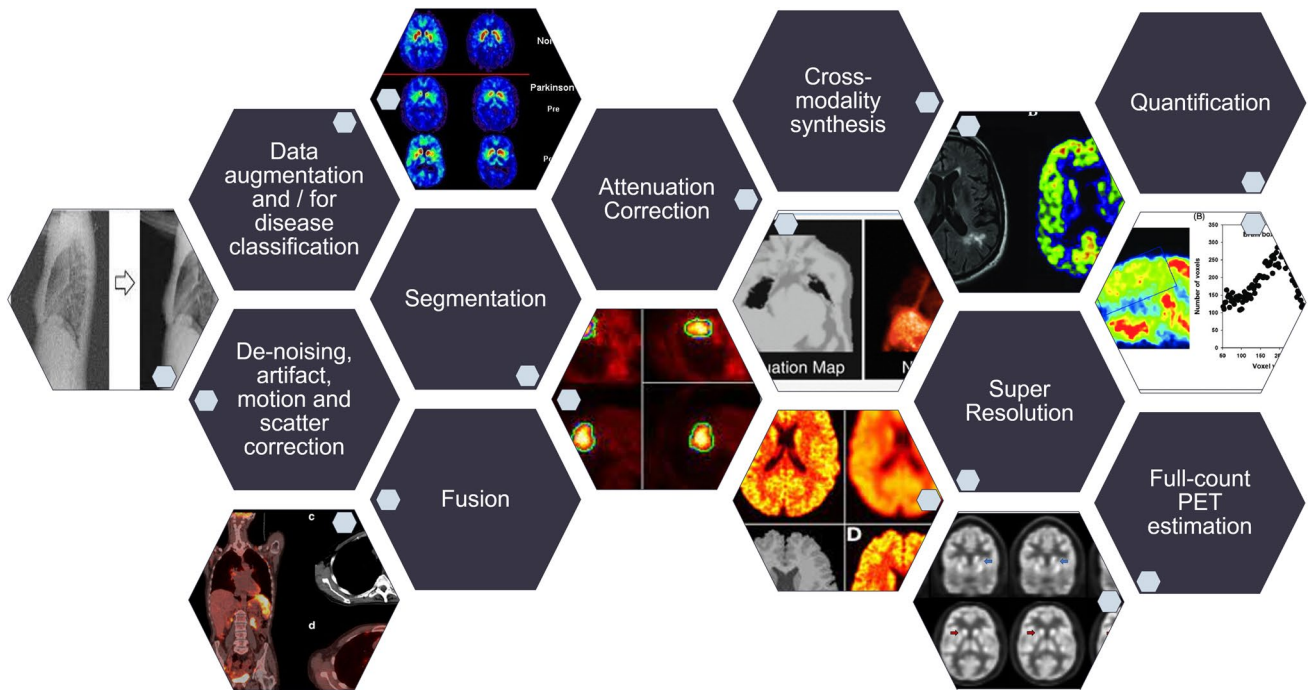


Fig. 4 GAN applications in PET imaging

GAN applications in Positron Emission Tomography

The applications were classified in the following 9 major fields.

Data augmentation and disease classification

Generating synthetic, unseen PET images from a set of authentic sources is a common task for GANs. The synthetic images can then be leveraged to increase the available

training sets and improve DL models in image segmentation, object detection, and classification. Although synthetic images are not real-case examples and may be of inferior quality to the original images in terms of tissue surroundings, edges and radiation information, they can facilitate an essential diversity among a training set and benefit a learning model [19]. Key papers focusing on data augmentation and disease classification using GANs are summarised in Table 1.

Table 1 Key papers focusing on data augmentation and disease classification using GANs

Reference Number	Purpose	Amount of training data	Results
[20]	Alzheimer's disease staging. GANs were used for data augmentation	411 PET Scans	The accuracy was improved by 10%
[21]	GANs were used for data augmentation	3471 slices	GANs are capable of estimating amyloid-positive and amyloid-negative SUVR images
[22]	Estimate future PET images for age-related disorders	256 PET scans	The estimated images showed great similarity with their actual counterparts
[24]	To predict post-treatment PET images from pre-treatment images	90 PET scans	Peak signal-to-noise ratio and a structural similarity index of 18.8 and 0.56, respectively, were reported
[23]	Feature extraction from Alzheimer's disease (AD) and normal cognitive (NC) scans	486 PET scans	Extracted features were helpful for AD and NC classification from various similar datasets from different sources
[27]	GANs were used for data augmentation	1200 PET scans	GANs synthesised dementia-related PET images successfully and improved the learning capabilities of the classification CNN

In the work of Islam and Zhang [20], a lightweight baseline GAN was developed to generate synthetic PET images from a set of real PET scans of the Alzheimer's disease domain to improve the classification accuracy among three predefined stages: normal controls (NC), mild cognitive impairment (MCI), and Alzheimer's disease (AD). As a result, the accuracy was improved by 10% when using the generated data in the training set. This methodology provides actual and synthetic brain PET images in Fig. 5.

In another study [21], the authors utilised a CycleGAN topology to synthesise additional amyloid PET scans training data for dementia detection based on standardised uptake values (SUVR). The results demonstrated that GANs could estimate amyloid-positive and amyloid-negative SUVR images.

In [22], GANs were used as part of a DL pipeline, generating future PET images based on PET scans at a certain time-point for age-related disorders, such as dementia. The proposed technique achieved a root mean square error of 2.5% and a peak signal-to-noise ratio of 32.6 dB using 3D-SSP images when predicting the image at 1 year from the baseline.

Kim et al. [23] used a boundary equilibrium GAN to classify Alzheimer's disease from PET images of two scanners. The authors used separate datasets for train and test to prove the efficiency of the proposed GAN in PET scanner variance. The proposed model achieved approximately 94% classification accuracy on both datasets, thereby confirming the effectiveness of the GAN-extracted features.

In another study [24], post-treatment PET images were generated by pre-treatment images to evaluate the patient's response to Hodgkin's lymphoma treatment. cGAN was proposed, reporting a peak signal-to-noise ratio and a structural similarity index of 18.8 and 0.56, respectively.

GANs have also been used to generate synthetic training data for Alzheimer's disease classification in other recent studies [25, 26].

A study by Noella et al. [27] deployed GANs to generate additional training images corresponding to several types of dementia. They furnished a deep CNN model, which discriminated among other dementia (OD), Alzheimer's and Parkinson's disease (AD and PD). The authors used 1200 PET images, achieving a classification accuracy of 97.7%.

PET image synthesis for data augmentation or disease classification purposes deploying GANs has also been reported in other relevant studies by Amyar et al. [28], Kang et al. [29], Bi et al. [30], and Cao et al. [31].

Attenuation Correction

PET detectors aim to detect the two emitted 511 keV photons after annihilating an emitted positron with a body electron. The tissues of the body absorb these photons as they travel through. Photon-tissue interaction also causes scatter. These lead to photon attenuation. Tissue thickness and electron density affect the degree of attenuation. This inherent PET phenomenon requires attenuation correction methods to generate the attenuation coefficient maps and create the AC image.

The corresponding CT images in hybrid PET/CT scanners provide the attenuation coefficient maps, which serve as transmission information to correct PET images. However, in PET/MRI systems, the MR images cannot serve as attenuation coefficient maps by themselves. In such cases, synthetic CTs (pseudo-CTs) can be generated from the corresponding MR images. GAN contribute a lot to this field. In recent research, Non-Attenuation Corrected (NAC) PET images are used to directly generate the sCT images by training DL algorithms with pairs of NAC-PET and the

Fig. 5 Real and synthetic brain PET images using the baseline GAN methodology. Reprint from [20] according to the publisher's open access policy

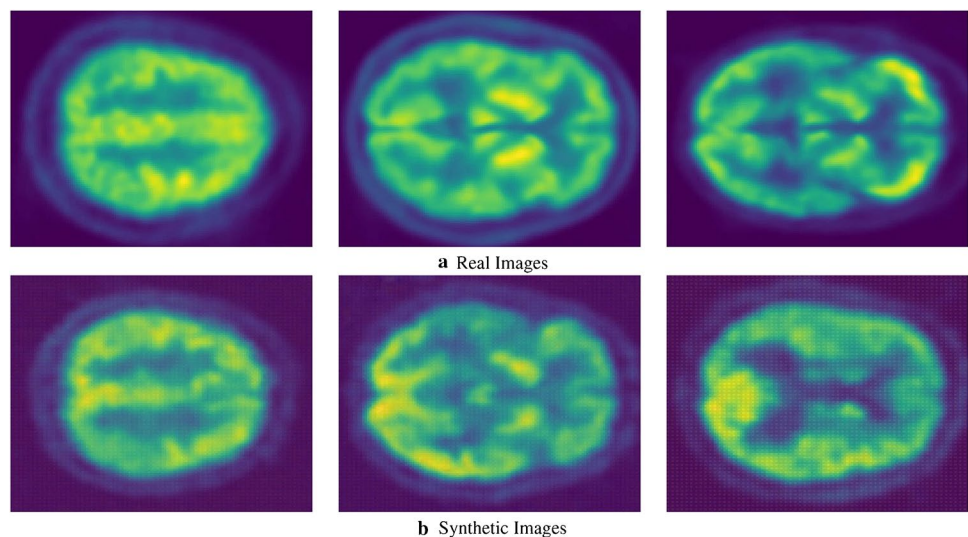


Table 2 Key papers focusing on PET image attenuation correction using GANs

Reference Number	Purpose	Amount of training data	Results
[32]	To synthesise the pseudo-CT image used for AC	50 MRI and PET scans	A mean standardised uptake value (SUV) bias of less than 4% in 63 brain regions was observed using the real CT-based attenuation corrected PET image
[33]	To generate the pseudo-CT images directly from NAC PET images	125 PET/CT scans	No major SUV deviations for most anatomic regions were observed between the synthetic and the authentic images
[34]	To generate the pseudo-CT images directly from NAC PET images	40 PET scans	High similarity metrics that demonstrated the effectiveness of Wasserstein GANs in estimating AC PET from NAC PET were reported
[35]	To generate the pseudo-CT images directly from NAC PET images	80 PET scans	Quantitative results suggested good similarity measures; however, vast variations in SUV uptake were observed
[36]	To synthesise the pseudo-CT image used for AC	20 PET scans	Less than 100HU difference between the real and the synthetic CT image and less than 1% mean quantification error between the synthetic AC PET and its true counterpart were observed
[38]	To synthesise the pseudo-CT image used for AC	10 PET scans	The overall average MAE of the pseudo-CT compared to the real CT test images was found to be 88.2 ± 32.7 HU

corresponding real CT images. Key papers focusing on PET image attenuation correction using GANs are presented in Table 2.

In the work of Arabi et al. [32], the authors developed an sCT generation algorithm based on deep learning adversarial semantic structure (DL-AdvSS). Two GANs were developed for synthesis and segmentation purposes. The segmentation stage separated the sCT image into four tissue classes: air cavities, soft tissues, bone, and background air. The MR image guided the framework into generating the pseudo-CT image, which was applied as an attenuation map to produce AC PET. The evaluation was based on 40-patient data under a twofold cross-validation process. A mean standardised uptake value (SUV) bias of less than 4% in 63 brain regions was observed using the real CT-based attenuation-corrected PET image.

Armanious et al. [33] proposed a framework to generate the pseudo-CT images directly from NAC PET images. The generator of the GAN topology consisted of four cascaded U-Net architectures, and the discriminator used the perceptual loss and the style content loss to identify the synthetic images. The authors used the GAN-generated pseudo-CT to construct the AC PET image. The GAN-generated CT and the corresponding AC PET were assessed qualitatively by visual inspection and visual analysis of colour-coded difference maps. Twenty-five whole-body PET scans were used for evaluation. In addition, quantitative analysis was performed by comparing organ and lesion SUVs. This showed no major SUV deviations for most anatomic regions; however, some deviations were identified in the diaphragmatic

lung border. An example of this study's results is given in Fig. 6.

Synthetic AC PET images and the corresponding pseudo-CT images could also be estimated directly from NAC PET data, as Hu [34] suggested in their work. They employed Wasserstein GAN to process the NAC PET data and produce the desired AC PET. NAC images were refined by removing noise and artefacts before network training. The authors reported high similarity metrics that demonstrated the effectiveness of Wasserstein GANs in estimating AC PET from NAC PET within an acceptable error range. In another work [35], the authors proposed Wasserstein GAN to directly obtain synthetic AC PET and synthetic T1-weighted MR images from NAC PET images corresponding to eighty patient scans containing head and neck data. Their framework removed artefacts and noise from the synthetic AC PET data to further estimate the MR counterpart. Quantitative results suggested good similarity measures; however, vast variations in SUV uptake were observed, possibly due to the denormalisation process, which was mandatory to estimate SUV values.

In Lei et al. [36], the authors used the CycleGAN topology to synthesise pseudo-CT (sCT) images from the NAC PET scans to estimate the AC PET. They evaluated their framework on 20 whole-body PET scans. The results showed less than 100HU difference between the real and the synthetic CT image and less than 1% mean quantification error between the synthetic AC PET and its true counterpart. In another study [37], the authors leveraged the MR images to construct the AC PET images using CycleGAN. Their

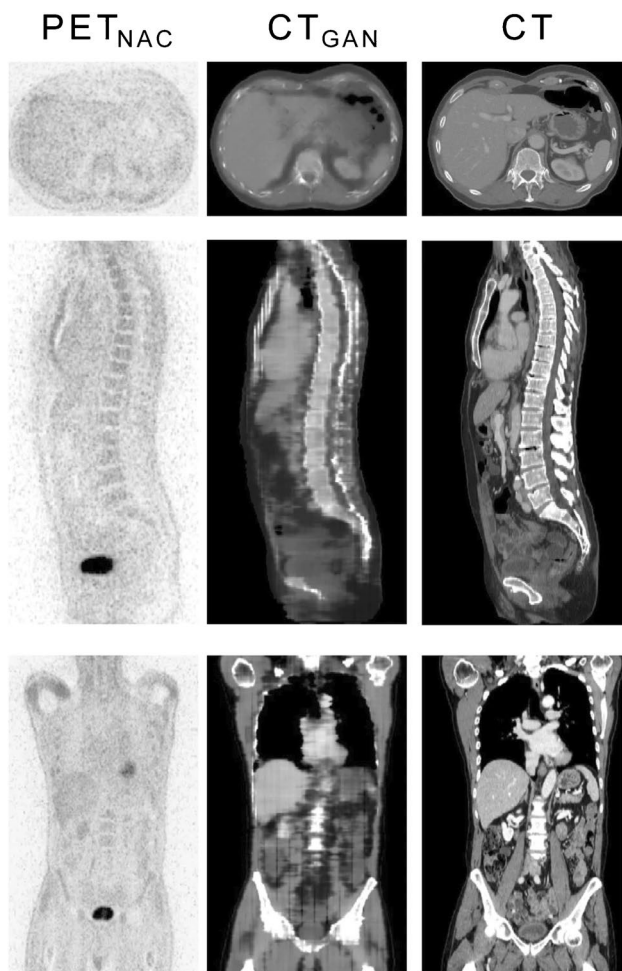


Fig. 6 Representative data set showing non-attenuation-corrected ^{18}F FDG-PET (left), generated pseudo CT (middle), and acquired CT (right) in axial (top), sagittal (middle), and coronal (bottom) orientation. CT_{GAN} data—while capturing the coarse distribution of CT anatomy—showed blurring and step formation in z-direction on coronal and sagittal reconstruction as well as irregular depiction of anatomical details. Reprint from [32] according to the publisher’s open access policy

proposal was evaluated on 18 patients’ datasets. This method showed a remarkable resemblance to the reference AC PET images, with a whole-body mean error below 0.1%.

Anaya and Levin [38] developed a successful CycleGAN framework to generate the pseudo-CT image from the MR image. The overall average MAE of the pseudo-CT compared to the real CT test images was 88.2 ± 32.7 HU. Similar tasks were successfully achieved in other relevant works [39–51].

Notably, the utilisation of GANs may offer the choice to bypass the CT-PET MR-PET data registration step due to those networks’ learning capabilities.

De-noising, Scatter correction and artefact removal

In addition, to the scatter correction mentioned previously, PET images suffer from noise and artefacts. Metallic implants, patient motion, contrast medium, and truncation typically produce image artefacts affecting the PET quantification procedure. In addition, clinical PET images often display increased noise levels compared to CT and MRI. Several methods have been developed to achieve noise reduction, scatter and motion correction, and artefact removal. For example, scatter correction is traditionally achieved by various methods, such as Monte Carlo simulation.

GANs have been recently deployed to perform image de-noising, motion correction and artefact removal in PET. To reduce noise, the generator network of the GAN topology is typically trained to estimate an equivalent image by its noise image counterpart. In MRI, maintaining structural information is essential. Similarly, maintaining the uptake information in PET is crucial for a successful de-noising and reconstruction. Key papers focusing on PET image de-noising, scatter, and artefact correction using GANs are reported in Table 3.

Geng et al. [52] used complementary learning to reduce CT, MR, and PET noise. They developed a content-noise complementary learning (CNCL) pipeline, which leveraged

Table 3 Key papers focusing on PET image de-noising, scatter, and artefact correction using GANs

Reference Number	Purpose	Amount of training data	Results
[52]	noise reduction in CT, MR, and PET	12 PET scans	Comparable or even superior results than several state-of-the-art de-noising methods were achieved
[53]	motion correction in noisy PET	10 PET/MRI scans	The absolute percentage difference between AUCs derived using the motion-corrected IDIF and the AIF was 1.2%
[56]	motion correction and de-noising of low-dose gated PET data	28 PET/CT scans	The proposed method could accurately generate motion estimation directly from low-dose gated PET images and produce high-quality motion-compensated low-noise PET reconstructions

the GAN topology to estimate the useful content of the input image by predicting the noise content. The network generator predicted the useful content and the noise of the input image separately. The discriminator, which is based on PatchGAN, is responsible for distinguishing between the real content and the generated content of the input image. The authors performed visual quality and quantitative tests and achieved comparable or even superior results than several state-of-the-art de-noising methods.

cGAN was used for motion correction in noisy PET scans by Sundar [53]. The performance of cGAN-aided motion correction was assessed by comparing the image-derived input function (IDIF) extracted from a cGAN-aided motion-corrected dynamic sequence with the AIF based on the areas under the curves (AUCs). The absolute percentage difference between AUCs derived using the motion-corrected IDIF and the AIF was 1.2%. The grey matter values determined using these two input functions differed by less than 5%. Du et al. [54] and Sundar [55] also reported effective employment of GANs for PET image de-noising and motion correction tasks.

In the study of Zhou [56], a developed framework called MDPET contributed to motion correction and de-noising of low-dose gated PET data. GANs were the cornerstone of the proposed methodology. Their results demonstrated that MDPET could accurately generate motion estimation directly from low-dose gated PET images and produce high-quality motion-compensated low-noise PET reconstructions (Fig. 7).

Low dose, Fast Scanning, sampling reduction

In PET imaging, it is desirable to reduce human body radiation exposure as low as reasonably achievable. Radiation exposure reduction requires a low dose PET scan with low-count PET emission data. Post-processing techniques, such as de-noising, are not efficient to estimate the full-count PET images. Firstly, the low-count PET noise is increased and is disparate from full-count PET noise. Secondly, the contrast-to-noise ratio increases, and, thirdly, uptake measurements are more biased. Low-count PET methods are, however, desirable and have applications in paediatric PET and radiotherapy response monitoring.

Pain and discomfort are typical patient issues that affect the produced artefacts due to motion, besides the patients' satisfaction. Whole-body PET scans require multiple bed positions to cover the entire body parts. Faster scanning is a conventional way to deal with this issue. However, a quick scan results in low-count PET data, which lack completeness compared to standard PET. Estimating full-count PET from low count statistics is a challenging task that GANs are useful in. Key papers focusing on PET image reconstruction following low-dose, fast-scan, or sampling reduction procedures using GANs are provided in Table 4.

Wang et al. [57] used 3D auto-context-based locality adaptive multi-modality generative adversarial networks model (LA-GANs) to estimate the full-dose FDG PET image from the low-dose counterpart and the accompanying MR. The results of the experiments, which were conducted on

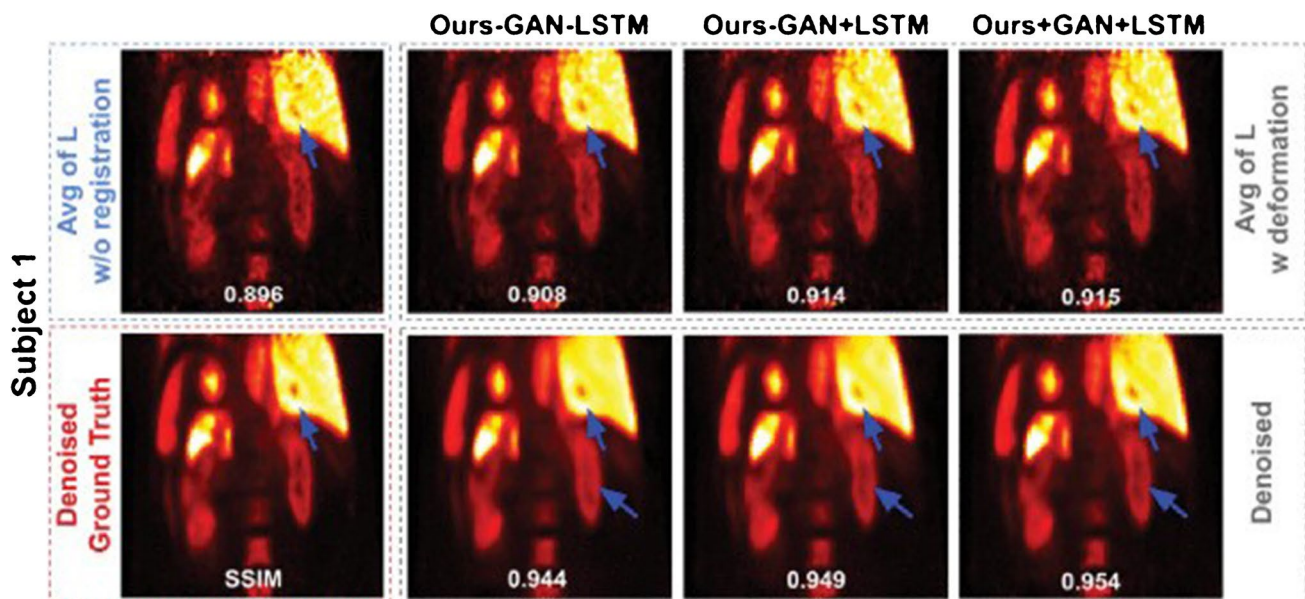


Fig. 7 A de-noising example of a low-dose gated PET. The averaged images L and the corresponding de-noised image from different MDPET configurations are shown in the 1st row and 2nd row.

Motion blurred anatomic structure is recovered using MDPET (blue arrows). Reprint and adapted from [55] according to the publisher's open access policy

Table 4 Key papers focusing on PET image reconstruction following low-dose, fast-scan, or sampling reduction procedure using GANs

Reference Number	Purpose	Amount of training data	Results
[57]	To estimate the full-dose FDG PET image from the low-dose counterpart and the accompanying MR	20 PET/MRI scans	The proposed method could effectively estimate full-dose FDG-PET images
[59]	To estimate the standard-dose FDG PET image from the ultra-low-dose counterpart	40 PET scans	This method achieved better results than the current best-performing strategy proposed by another study [60]
[73]	To estimate the standard time PET of ~ 27 min from a fast-scan PET of ~ 3 min	100 PET scans	The average SUV bias among the estimated PET and the actual image calculated over normal tissues was $3.39 \pm 0.71\%$
[74]	To reconstruct 20-min standard time scanning PET (PET20m) from the corresponding 2-min standard time PET (PET2m)	294 PET scans	Although mean uptake differences were observed between the synthetic PET20m and the real PET20m images, similarity measures yielded remarkable results
[78]	Low-dose and/or fast-scan PET image reconstruction	25 PET scans	The average mean error and normalised mean square error in the whole body were $-0.14\% \pm 1.43\%$ and $0.52\% \pm 0.19\%$ with CycleGAN model, compared to $5.59\% \pm 2.11\%$ and $3.51\% \pm 4.14\%$ on the original low count PET images
[79]	PET reconstruction from sinogram data	7 PET scans	The reconstruction results of the proposed method are highly consistent with the ground truth in both terms of sharp edges and high pixel values of ROIs

both real human and phantom brain datasets, revealed that the proposed method could effectively estimate full-dose FDG-PET images. Moreover, this method was superior to traditional multi-modality fusion alternates and other state-of-the-art PET estimation approaches in qualitative and quantitative metrics. In a study by a similar research team [58], the authors proposed a 3D cGAN framework to estimate full-dose FDG PET from solely the low-dose PET data without utilising the MR modality.

In another work [59], ultra-low-dose PET images were reconstructed to represent standard-dose images using cGAN. This methodology used 39 participants for evaluation and achieved better results than the current best-performing strategy proposed by another study [60]. Those results were superior by 1.87 dB in PSNR, 2.04% in SSIM, and 24.75% in RMSE [60].

Recent works have also studied estimating standard-dose PET images from low-dose or ultra-low-dose PET employing mainly CycleGAN topologies [61–72].

Sanaat et al. [73] developed a CycleGAN topology to estimate the standard time PET of ~ 27 min from a fast-scan PET of ~ 3 min. Their methodology was evaluated using one hundred patient cases. Two nuclear medicine physicians assessed the quality of the generated images. In contrast, the diagnostic quality of the predicted PET images was evaluated using a pass/fail scheme for the lesion detectability task. Quantitative analysis using established metrics including standardised uptake value (SUV) bias was performed for the liver, left/right lung, brain, and 400 malignant lesions from the test and evaluation datasets. CGAN scored 4.92 and 3.88 (out of 5) for brain and neck + trunk, respectively. The average SUV bias calculated over normal tissues was $3.39 \pm 0.71\%$. The Bland–Altman analysis reported the lowest SUV bias (0.01%) and 95% confidence interval of $-0.36, +0.47$ for CGAN compared with the reference images for malignant lesions.

In the work of Jeong et al. [74], it was proved that fast-scanning setbacks in the corresponding texture and image quality of amyloid PET images could be overcome by reconstruction based on GANs. The authors employed a DC-GAN to reconstruct 20-min standard time scanning PET (PET20m) from the corresponding 2-min standard time PET (PET2m). Although mean uptake differences were observed between the synthetic PET20m and the real PET20m images, similarity measures yielded remarkable results and implied that future research could further improve the results (Fig. 8).

Similar results were also reported in three related studies by Sanaat et al. [75], Kim et al. [76], and Xue et al. [77].

In addition, low-count PET (either low-dose or fast scan) transformation was also reported in the study of Lei et al. [78]. The cycle GAN topology was implemented to synthesise diagnostic PET images using low count data. The

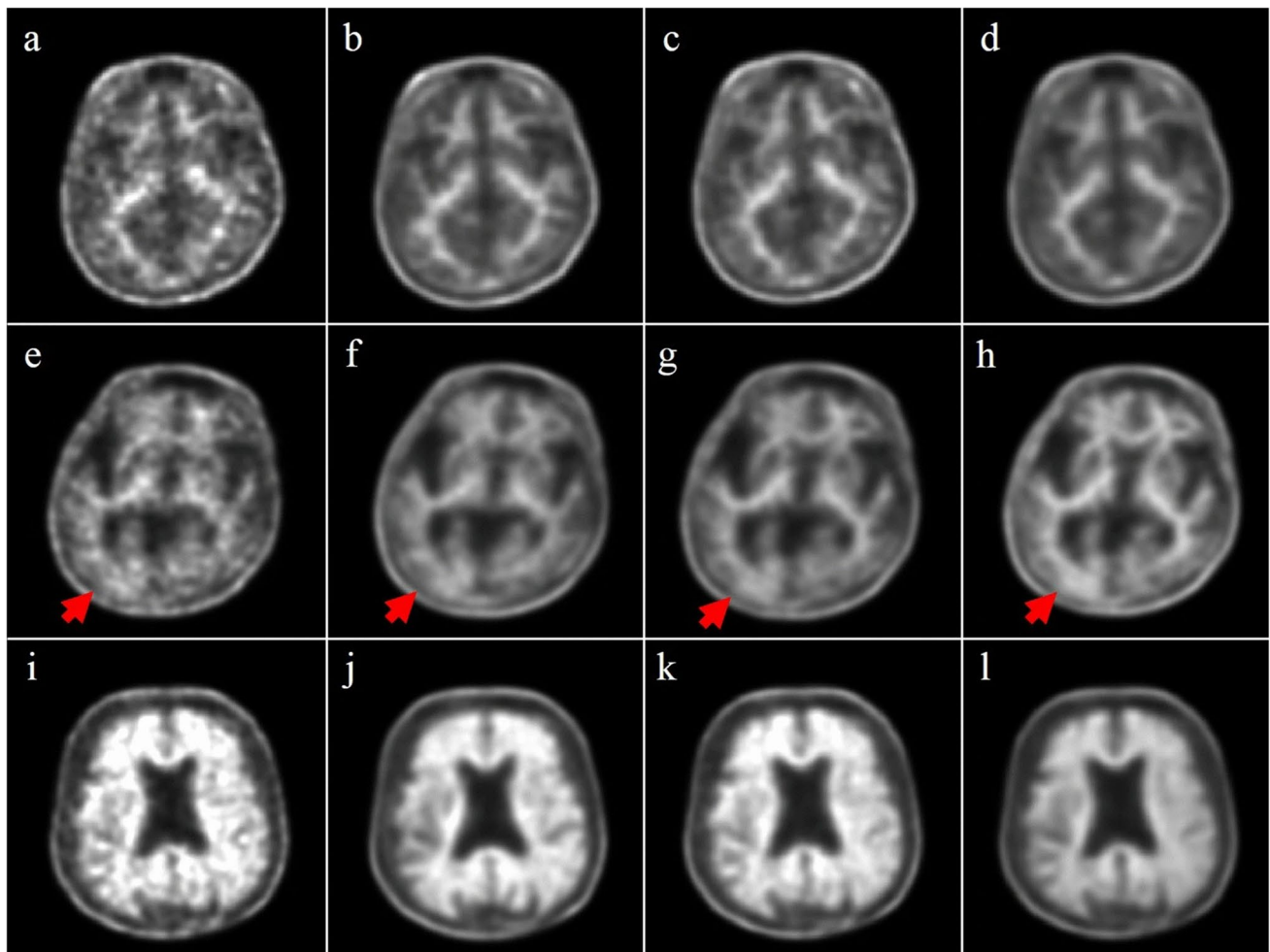


Fig. 8 An example of fast-scan PET image reconstruction. The input and output of PET images (upper row, BAPL 1; middle row, BAPL 2; lower row, BAPL 3) are shown here. PET2m image (input image) is very noisy, and the image quality is poor (a, e, i). The ground truth with 20-min scanning (b,f,j) and synthetic PET images generated from the proposed deep learning (c,g,k) and the U-net (d,h,l) are

shown. The synthetic PET image generated from our model is better in reflecting the underlying anatomical details than is the PET image generated from the U-Net. In the BAPL 2 case, a small positive lesion (red arrows, e–h) is equivocal in the PET2m image (e), but clearly shown in sPET20m image (g) as in PET20m image (f). Reprint from [72] according to the publisher’s open access policy

average mean error and normalised mean square error in the whole body were $-0.14\% \pm 1.43\%$ and $0.52\% \pm 0.19\%$ with Cycle GAN model, compared to $5.59\% \pm 2.11\%$ and $3.51\% \pm 4.14\%$ on the original low count PET images. Normalised cross-correlation is improved from 0.970 to 0.996, and the peak signal-to-noise ratio is increased from 39.4 dB to 46.0 dB with the proposed method.

PET reconstruction from sinogram data was achieved by Liu et al. [79] using the cGAN framework. They tested their approach against Monte Carlo simulated PET reconstructed data and real PET cases. The reconstruction results of this method were highly consistent with the ground truth in both terms of sharp edges and high pixel values of ROIs.

Super-resolution

Super-resolution (SR) is the domain wherein a high-resolution image is synthesised by a low-resolution source. The conventional method requires increasing the original image size and using interpolation and filtering methods to enhance it. The conventional methods may result in heavier noise. GANs use low-resolution images and learn to learn patterns that transform regions of low resolution to superior quality.

In the study of Song et al. [80], which extended former relevant work [81], the high-resolution anatomical MR image and the low-resolution functional PET image were combined to generate a high-resolution PET image preserving both anatomical and functional characteristics.

Two CycleGAN-based generators were used to estimate the high-resolution PET and map this image back to the low-resolution counterpart. Twelve scans were used as a validation set from a dataset of 30 scans. The evaluation metrics (PSNR, SSIM, CNR, and NRM-SR) confirmed the assumption that GANs can be of use in super-resolution PET image generation.

Segmentation

Attention has to be paid to specific human body areas in many situations. Medical imaging provides the complete visualisation of larger areas. In such cases, quantification of the findings is impossible without delineating the objects of interest or the entire regions of interest. Segmentation refers to the delineation of such boundaries in images. Tissues, organs and tumours are typical segmentation targets. Manual segmentation is time-consuming and subjective. Usually, GANs are accompanied by traditional segmentation models in the pipeline. However, in some works, GANs are used to estimate the segmentation map, an auxiliary binary image that enables segmenting the original. GAN-based methods were superior to the traditional U-Net-based approaches in most reported studies.

White matter hyper-intensities (WMH) are traditionally segmented using MR modality because WMH is not visible on FGD-PET. In a recent study [82], the authors developed a cGAN to segment and estimate WMH from ^{18}F -FDG PET scans. In the study, Pix2pix GAN is developed to generate the segmentation map used to apply the segmentation. The authors compared the predicted PET WMH volumes with the ground truth obtained by MRI to achieve the volume estimation. The dice similarity coefficient (DSC), recall, and average volume differences (AVD) were used as evaluation metrics. The authors compared the performance of cGAN with H-Dense U-Net, which is commonly used for segmentation tasks. cGAN outperformed H-Dense U-Net

for volume estimation, yielding excellent correlation coefficients. Similar results were reported in the study by the same first author [83].

GANs have also been used for tumour segmentation in recent studies by Wu et al. [84] and Yousefirizi et al. [85]. In the study of Wu et al. [84], the authors developed an adversarial encoder-generator network, which estimates the normal PET image from PET images containing lung tumours and nodules. The residual map, the difference between the real PET images and the learned normal PET images, is then used to segment the findings. The authors compared their method with the traditional U-Net CNN and other reputable methods, such as the variation auto encoders and reported better results in terms of dice coefficient (achieving 0.620), sensitivity (0.779), and specificity (0.999).

Yousefirizi et al. [85] proposed a GAN network to segment head and neck tumours from PET scans. The proposed GAN estimates the binary image that serves as a segmentation map. The authors reported better results compared to the conventional U-Net methodology. More specifically, the mean dice similarity measure is observed to be 69% (with U-Net achieving 62.3%), and the precision is found to be 78% (with U-Net achieving 62.6%).

Fusion

Image fusion in PET imaging aims to combine the functional information provided by the PET image and the structural information provided by other modalities, such as CT and MRI, into a single image. In PET/CT image fusion, the generated study can demonstrate abnormalities that cannot be identified by either CT or PET images alone. A limited number of studies reported the successful application of GANs in medical image fusion, specifically in PET.

Ma et al. [86] achieved PET and MRI image fusion by proposing a novel modification of cGAN, which contained two discriminators aiming to distinguish between synthetic

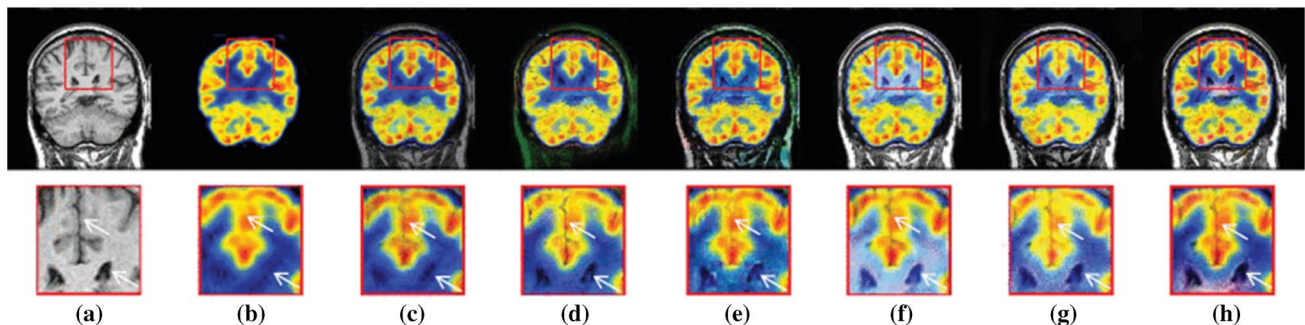


Fig. 9 An example of PET and MRI fusion from [85]. (a) MRI image; (b) PET image; (c) result using IHS-Retina method; (d) result using non-subsampled shearlet transform method; (e) result using low-rank sparse dictionaries learning method; (f) result using non-

parametric density model; (g) result using CNNs; (h) result using proposed method. Reprint from [85] according to the publisher's open access policy

fused images and their authentic counterparts. Their proposal was validated on the publicly available Harvard medical school website.

Kang et al. [87] proposed a cGAN-based network to combine PET and MRI images and generate a fused outcome (Fig. 9). The proposed discriminator was designed to urge the generator network to synthesise fused images containing more structural information from the MRI images and more functional information from the PET images. The generator network was developed based on U-Net. They compared their results against conventional and CNN-based methods in terms of the entropy, the average gradient, the spectral discrepancy, and the $Q^{AB/F}$ measures. Their method was found superior to the selected techniques.

In two similar related works by Huang et al. [88] and Yang et al. [89], the authors reported acceptable fusion results implementing CycleGAN topologies.

Evaluation of quantifiable PET parameters

There are few studies evaluating the applications of GANs in calculating quantitative parameters of PET studies. These studies mainly deal with quantifying amyloid uptake in corresponding PET brain studies. Furthermore, there is a scarcity of such studies evaluating typical parameters of oncological PET such as tumoural Standardised Uptake Values (SUVs), Metabolic Tumour Volumes (MTV), or Total Lesion Glycolysis (TLG).

Non-specific uptake refers to a situation where the observed uptake reflects non-specific clinical importance and can't be recognised and properly categorised. Liu et al. [90] compared CNNs and cGAN to remove the undesirable non-specific (NS) uptake from the amyloid PET measurement, which biases the standardised uptake value ratio (SUVr) used to quantify amyloid- β burden from amyloid-PET scans. The cGAN topology was employed to map structural MR to NS PET images. The cGAN model

was competent with the equivalent CNN architectures for this task. Key papers focusing on PET quantification using GANs are summarised in Table 5.

Image-to-image translation between diverse PET scanner technologies is useful in estimating cortical amyloid load and circumventing the incomplete interchangeability of various radiotracers, which prevents long-term clinical trials. Kang et al. [91] trained a CycleGAN framework to translate C-11 PIB and F-18 florbetapir (AV45) PET scans and discover a specific uptake pattern to estimate SUVr regardless of the scanner. The results showed that the specific uptake was well-recovered by the CycleGAN pipeline yielding minor errors in SUVr quantification. Finally, in work by Kang et al. [92], the authors studied the spatial normalisation (SN) of amyloid PET images for Alzheimer's disease assessment without the need for co-registered MR images. They trained a GAN with MR images and PET images in the 3D format. They developed a framework that successfully estimates the spatially normalised 3D PET image using the transformation parameters obtained from MRI-based SN.

Estimation of Non-specific Uptake in Amyloid-PET Images based on MRI modality, which serves the purpose of amyloid load quantification in Alzheimer's Disease [93]. The proposed cGAN was trained to learn the mapping between the MR and non-specific PET images. The generated non-specific PET images were compared to the real PET scans, achieving a mean SUVr difference of 1.90% in the grey matter.

In a study by Ma [94], online dose verification based on proton-induced positron emitters was achieved using a DiscoGAN framework. This framework was tested on five reconstructed PET images based on an in-beam PET system and a spread-out Bragg peaks (SOBPs) dataset. The mean relative error of the centre lines was < 3% (under signal-to-noise ratio), and the range uncertainty was < 1 mm.

Table 5 Key papers focusing on PET quantification using GANs

Reference Number	Purpose	Amount of training data	Results
[90]	To remove the undesirable non-specific (NS) uptake from the amyloid PET measurement	172 PET/MRI scans	The cGAN model was competent with the equivalent CNN architectures for this task
[91]	To translate C-11 PIB and F-18 florbetapir (AV45) PET scans and discover a specific uptake pattern to estimate SUVr regardless of the scanner	681 PET/MRI scans	The specific uptake was well-recovered by the CycleGAN pipeline yielding minor errors in SUVr quantification
[93]	To Estimate Nonspecific Uptake in Amyloid-PET Images based on MRI modality	40 PET scans	The generated non-specific PET images were compared to the real PET scans, achieving a mean SUVr difference of 1.90% in the grey matter
[94]	Online dose verification based on proton-induced positron emitters	900 dose vs activity pair	The mean relative error of the centre lines was < 3% (under signal-to-noise ratio), and the range uncertainty < 1 mm

Cross Modality Synthesis

Cross modality synthesis in PET imaging refers to a set of methods to synthesise CT from PET, PET from CT, MRI from PET, and PET from MRI. This topic in the field of computer vision is also called image-to-image translation. The reader should note that the aim is to estimate the corresponding modality from another modality in this domain, without any other information.

Cross-modality synthesis is a very controversial topic because each imaging modality captures unique information that the others inherently can't. For example, moving from a functional image (e.g. PET) to a structural modality (e.g. CT) is hypothetically easier than the vice-versa [12]. But, on the contrary, estimating the PET modality's functional information from the CT modality's structural information is inherently very challenging, if not impossible.

Although the PET imaging method captures functional information that is unique compared to other modalities, an experienced radiologist or nuclear medicine can often conceive the expected findings of the PET scan based on the MRI counterpart and historical clinical data. It is highly

unlikely that a DL network would manage to achieve PET image synthesis from solely MRI images and clinical information, although it is an application worth exploring.

The availability of different modalities can improve medical diagnosis and treatment suggestions. In this area, the composition of one or the other modality can help significantly, given that the images complement each other. The synthetic image is not absolved from errors and does not precisely reflect reality. Still, it may approach reality to an acceptable limit, which depends on the purpose of the study. Cross-modality synthesis using GANs could be beneficial for quantifying important features in the absence of the PET modality, imputing or augmenting the available data for lesion, bone, and tissue segmentation and fusion tasks, and reducing the false-positive findings for detection tasks. However, the importance of those applications, the precision, and the suitability of GANs in cross-modality synthesis is constrained by the fact that different modalities display findings of different nature that do not necessarily correspond to or interfere with each other. Key papers focusing on PET cross-modality synthesis using GANs are reported in Table 6.

Table 6 Key papers focusing on PET cross-modality synthesis using GANs

Reference Number	Purpose	Amount of training data	Results
[95]	T1-weighted MR to FDG-PET image synthesis	15 PET/MRI scans	The results suggest the potential interest of encouraging the preservation of gradient energy in the brain for MR to PET translation GANs
[96]	To generate virtual PET images from their MR counterparts	680 PET/MRI scans	The synthetic PET images could be useful for image segmentation and fusion activities, despite their lack of functional information
[97]	To predict the PET-derived myelin content map from the multi-modal MRI	12 PET/MRI scans	The proposed method could obtain similar measures to the PET-derived ground truth at both global and voxel-wise levels
[98]	To impute the missing MR data from incomplete pair MRI and PET scans	2355 PET/MRI scans	HGAN could successfully synthesise reasonable neuroimages and achieve promising results in brain disease identification
[110]	To estimate MR images from amyloid PET	261 PET/MRI scans	The generated MR images from florbetapir PET showed visually similar signal patterns to the real MR
[111]	To achieve image-to-image translation between PET and CT	46 PET/CT scans	MedGAN produced realistic and homogeneous bone structures in the resultant CT images that closely matched the ground truth CT images and surpassed visually those produced by related studies
[114]	To generate PET-like images from CT	23 PET/CT scans	The synthesised PET is shown to improve an existing automatic lesion detection software by reducing the false positives by 28%
[119]	To predict post-treatment PET scans from their corresponding SPECT and CT	19 PET/CT and SPECT scans	The comparisons between the real and the synthetic/predicted PET/CT scans showed an average absorbed dose difference of $5.42\% \pm 19.31\%$ and $0.44\% \pm 1.64\%$ for the tumour and the liver area, respectively

PET from MRI In the work of Hognon et al. [95], the authors proposed the pix2pix method with adversarial, gradient difference and pixel losses for T1-weighted MR to FDG-PET image synthesis. Furthermore, they used the average root mean squared error and structural similarity SSIM between the synthetic the simulated FDG images for quantitative assessment of their models. The results suggest the potential interest of encouraging the preservation of gradient energy in the brain for MR to PET translation GANs. An example of such an application is given in Fig. 10.

Hu et al. [96] proposed a bi-directional mapping GAN generate virtual PET images from their MR counterparts. They evaluated their model on 680 subjects of an Alzheimer's disease dataset, which includes pairs of MR and PET images. In addition, the authors benchmarked several traditional GAN topologies to compare their results and proved that their model produced more realistic PET images. Although PET images are synthesised in a non-deterministic way, and the functional information of the actual PET scan cannot be determined or estimated by the MR modality, the synthetic PET images could be useful for image segmentation and fusion activities.

In another study [97], the authors developed a GAN-based method to predict the PET-derived myelin content map from the multi-modal MRI. They aimed to measure the tissue myelin content used to examine multiple sclerosis without PET data. The authors furnished a Sketcher-Refiner GAN. The results showed that the proposed method could obtain similar measures to the PET-derived ground truth at global and voxel-wise levels.

Pan et al. [98] proposed to impute the missing MR data from incomplete pair MRI, and PET scans to construct an adequate dataset for brain disease diagnosis based on multi-modal data. They proposed a hybrid GAN (HGAN) topology

that learns to synthesise MR data by training on pairs of MR and PET sets. Three databases were used to evaluate this methodology, with the results verifying that HGAN could successfully synthesise reasonable neuroimages and achieve promising results in brain disease identification.

The applications of GANs in MR-to-PET image translation serve tasks such as image imputation (where the PET image is missing), PET image estimation for quantification purposes, and PET image synthesis for other purposes. Mainly brain MRI modality is thoroughly examined for MR-to-PET translation deploying various GAN topologies, such as CycleGAN in several related studies [99–104]. GANs find application in Alzheimer's disease detection and staging in other research studies [105–109].

MRI from PET Construction of MR images from amyloid PET was studied in the work of Choi et al. [110]. The authors adopted the cGAN topology to generate the MR images. The quantification of the cortical amyloid load was used as a reference standard to inspect the effectiveness of the proposed framework. PET images were spatially normalised to the template space using the generated MR. Then, standardised uptake value ratio (SUVR) of the target regions was measured by predefined regions-of-interests. Generated MR images from florbetapir PET showed visually similar signal patterns to the real MR. The structural similarity index between real and generated MR was 0.91 ± 0.04 . The mean absolute error of SUVR of composite cortical regions estimated by the generated MR-based method was 0.04 ± 0.03 . The particular application of GANs was the only one found in the literature search by the end of 2021.

CT from PET Armanious et al. [111] used a similar methodology described in [33] to propose a multi-purpose framework that performs image-to-image translation between PET

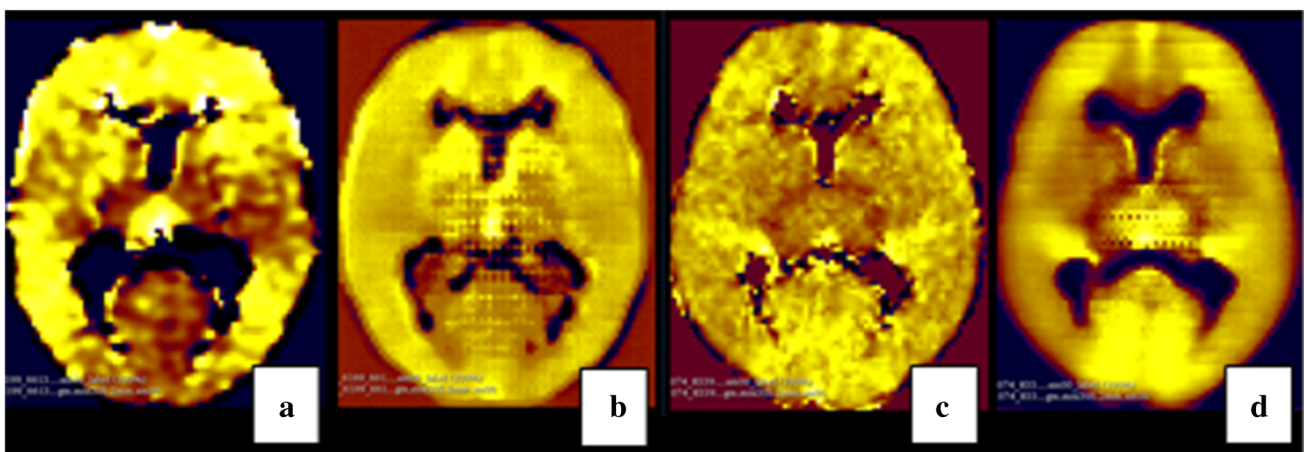


Fig. 10 An example of PET from MRI synthesis from [98]. Examples of actual $^{18}\text{F-AV1451}$ PET and $^{18}\text{F-FDG}$ PET (a, c) images and the synthesised (b, d) images. Reprint from [98] according to the publisher's open access policy

and CT, MR motion artefact correction, and PET image denoising. They named their framework MedGAN. MedGAN produced realistic and homogeneous bone structures in the resultant CT images that closely matched the ground truth CT images and surpassed visually those produced by related studies.

Santini et al. [112] and Sharma et al. [113] also reported successful CT from PET vice-versa image translation using GANs.

PET from CT Although synthesising a PET image directly from a CT image sounds worthless of the effort, a study by Cohen [114] suggested that generating PET-like images would be helpful for a false-positive reduction in lesion detection, mainly when focused on malignant lesions in the liver. The authors employed cGAN for this task. The synthesised PET is shown to improve an existing automatic lesion detection software by reducing the false positives by 28%. Other studies investigated the possibility of estimating the corresponding PET from its CT equivalent either for PET quantification (FDG uptake—metabolic activity) or for other diagnostic tasks (e.g. progression) in related studies [115–118].

Plachouris et al. [119] investigated the role of GANs in predicting post-treatment PET scans from their corresponding SPECT and CT counterparts in patients with liver cancer who underwent radioembolisation with ^{90}Y microspheres. They developed an innovative 3D voxel-based variation in the Pix2Pix model for the particular task. The comparisons between the real and the synthetic/predicted PET/CT scans showed an average absorbed dose difference of $5.42\% \pm 19.31\%$ and $0.44\% \pm 1.64\%$ for the tumour and the liver area, respectively.

Discussion

The current review evaluated the recent literature in the domain of PET with the deployment of GANs. As discussed above, almost every image processing operation in PET may be performed by GANs or by hybrid DL methods, incorporating GANs. Several GAN topologies have been deployed in the latest research, as the current review revealed (Fig. 11).

The utilisation of GANs in PET imaging can circumvent crucial setbacks derived from the conventional methods. By applying GANs, image generation is no longer dependent on naïve geometrical and texture deformations, which emerge by tuning well-known image features. Furthermore, synthetic images produced by GANs have no obvious similarity with the images used to train the discriminator because the

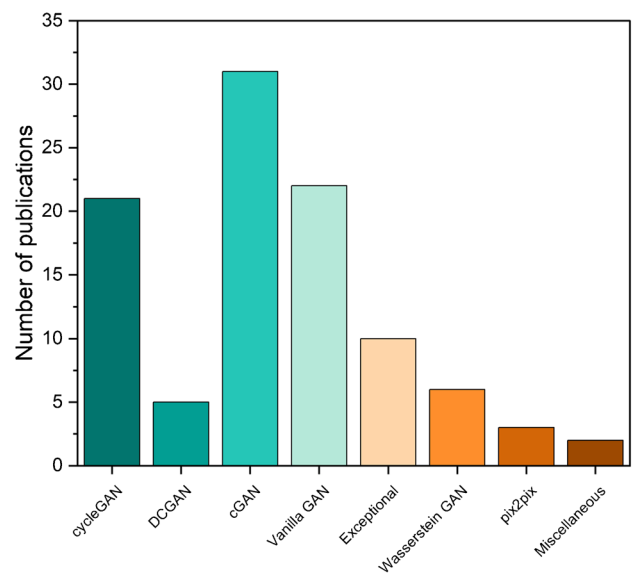


Fig. 11 GAN topologies found in the literature review

original images are unseen to the generator. Instead, GAN depends on feature extraction to identify the domain space of the desired output data distribution and can ideally generate data points that maintain the essence of the training data rather than reproducing the same material with minor alterations. This is an important and desirable outcome. For example, we prefer a model to evaluate a lung nodule, how it is defined in space, and the unique characteristics that identify it as a nodule and not as another tissue. A model that can capture this knowledge from training data is considered robust, multi-functional, and reasonable.

GANs base their structure in CNNs, which are inherently able to ignore spatial differences among images and generalise into space. This capability enables CNNs to map the input images to feature abstract information spaces rather than follow a pixel-to-pixel approach. In medical imaging, this advantage could be useful for bypassing the registration step when examining images of different modalities or volumetric data derived from 2D slices.

The most powerful characteristic of GANs is their inherent ability to seek and reveal a transfer function transforming the input data of one domain to the desired data of another domain and vice-versa. This is particularly beneficial in image-to-image translation. In medical imaging, multi-modality diagnosis is an everyday clinical routine. GANs could successfully remove noise from low-dose images and estimate their standard-dose counterparts. They discover the necessary transfer function, which eliminates the noise while maintaining anatomical and functional information. The versatility and the modality-independent applicability of GANs make them a powerful option for such tasks.

Another application is that of the attenuation correction. GANs could pave the way to reconstructing AC PET images solely from NAC PET, even without the auxiliary information of an MR or a CT image. We argue that the estimated AC could still significantly impact diagnosis despite the information loss in this process. Similar to the latter examples, super-resolution, scatter correction, and even segmentation can be achieved by GANs, as already discussed. Before GANs, such tasks were still possible to perform using non-automatic methods. GANs could potentially replace such methods due to their efficiency and inherent ability to perform automated image processing without further supervision.

In the reported studies, GAN-based methods were applied domains where conventional CNN methods and other techniques are already dominant. Nevertheless, GANs demonstrated superior results in specific tasks (e.g. segmentation).

Limitations

GANs still face limitations and functional issues that require improvements. Their dependency on large-scale datasets poses challenges, as available imaging data are often insufficient to exploit the capabilities of high-performance computing clusters that could host large-scale GAN training campaigns. At least, for most of the research community, medical imaging data are constrained to a few thousand in amounts. Despite the good results even with these datasets, they cannot ensure accountability and effectiveness of GANs in immediate everyday action. In addition, detailed annotations and accurate labels are mandatory for GANs or similar DL methods to operate. This procedure is time-consuming and nontrivial, especially when dealing with very small tissues requiring delineation. Nevertheless, the use of CycleGAN can alleviate this obstacle, at least in the domain of image-to-image translation, because it requires fewer registered images from the two domains.

Training of GANs is a complex topic, as there is always the possibility of mode collapse, vanishing gradients, and failure to converge. The vanishing gradient issue refers to a state of the discriminator being too effective in distinguishing between synthetic and authentic images. The generator is not capable of learning in depth, leading to training failure. The Wasserstein and the Modified minimax loss functions are suggested to overcome this issue; however, the problem has not been solved effectively. Mode collapse refers to a situation where the generator repeatedly outputs the same result, forcing the discriminator to reject the outputs. This can affect the discriminator's robustness while the generator gets better and easily "deceives" the discriminator when the outputs are changed. This process leads the generator to rotate over specific outputs in an attempt to "trap" the discriminator. The result is that the GAN is no longer producing

useful diverse images. Failure to converge is a typical issue and describes a situation where the discriminator fails to find the correct pattern to distinguish between synthetic and authentic inputs, thereby dropping its accuracy to 50% (the random guess).

Another issue arises when task-specific GANs are designed. Usually, complex GAN topologies utilise more than one loss component in the loss function. For example, besides the adversarial loss, CycleGAN uses the cycle consistency loss. Some of the referenced studies utilise more than two loss components. This phenomenon makes the optimisation problem even more challenging.

Most studies commonly face the above issues in GANs for any task and are usually circumvented by extensive experiments, sophisticated approaches and topology modifications, or parameter tuning. Carefully designing the architecture, the knowledge capacity, and the parameters of both the generator and the discriminator for a specific task may require days and even weeks of training. Although GANs require less supervision and less time to perform the desired task when compared to manual procedures, they require much attention during their development stage. Moreover, initial training and future re-training to remain up to date increase computational costs.

Employing GANs to improve the signal quality or to estimate missing information (as it happens in attenuation correction, fusion, and cross-modality synthesis) might obscure the presence of real pathology. Furthermore, several studies report the phenomenon of image hallucinations [120], which refers to the generation of unusual and irrelevant image features, such as false, unexplainable structures. For example, a minor image hallucination may be a slight imperfection when reconstructing tissue boundary. In contrast, an important hallucination may refer to introducing an entirely new structure in the image.

Privacy and fraud issues may even arise in applications with GANs. Their capabilities in generating fake images indistinguishable from legitimate images may enable their use for medical fraud. GANs enable the complete synthesis action and placement of fake findings such as aneurysms, torn ligaments or tendons, and tumours in the medical image. In [121], the authors present such potential dangers that tampering with CT scans and artificially injecting lung cancers on those images with DL methods managed to deceive the radiologists at least 70% of the time.

Another vital issue is the explainability of such networks. GANs are deep CNNs, which learn to map the input data distribution into the abstract feature space by applying several filters and performing massive amounts of mathematical operations in no time. GAN's trainable parameters may vary from a few thousand to millions. Tracking the cognitive process to gain insights on the decision-making of such frameworks is a very complex and ambiguous topic that attracts

the interest of many research studies. DL frameworks are often called black-boxes due to the above fact, making medical experts reluctant to employ such systems in everyday activities.

Finally, assessment metrics vary between studies. Image quality and image similarity measures include dice similarity measure, mean absolute error, peak signal-to-noise ratio, structural similarity, and more. The physician's quality assessment is employed in many cases, but it is subjective. There needs to be standardisation to avoid subjective conclusions and establish comparison guidelines.

Future perspectives

Apart from fundamental research on improving the core of GANs to surpass the inherent limitations mentioned above, specific attention by biomedical engineers and physicians should be paid to the applicability of GANs in medical imaging.

A severe issue is data scarcity. PET imaging modality is under-represented in most medical imaging record archives and initiatives by institutes and laboratories. Without utilising large-scale, complete, and well-structured PET imaging data covering a variety of diseases apart from the common ones, future research will be constrained.

Despite the effectiveness of general GAN topologies, such as CycleGAN and cGAN, more research could be conducted to design, develop and evaluate task-specific or model-specific topologies, architectures and components. Those models can potentially enhance the robustness of GANs in medical imaging and direct the research towards discovering methods and materials that apply to problem-specific GAN topologies. These models could also integrate clinical data and attributes to expand their learning efficiency and capture general knowledge about the discovered patterns and objects in the images. This aspect could also contribute to the explainability issue, as clinical data can be used as auxiliary information that could guide the model to a specific and desired path, thereby offering some control over the internal operations of such networks. In addition, clinical data, in conjunction with output GAN features, could be processed by more transparent methods, such as Random Forests and Fuzzy Cognitive Maps, to improve the model's explainability as a whole.

GANs also need to be applied to various PET scanners to assess their robustness to device variation. Ideally, a universal GAN model should be developed to handle PET image data regardless of the PET scanner variations for a specific task (e.g. artefact removal). However, recent studies suggest that DL methods are proved to be excellent in acquisition device variation [122, 123], and GANs could be no different.

Conclusions

This review analysed research studies focusing on GANs in PET imaging between 2015 and 2021. More than a hundred related researches were examined and discussed. GANs have enjoyed significant research attention to medical imaging related tasks during the last two years. PET imaging is a domain wherein extensive research has only begun after 2019. Nevertheless, GANs find application in several PET imaging processes, such as attenuation correction, standard-dose image estimation, scatter correction, artefact removal, noise reduction, image fusion, and cross-modality synthesis. The reported results verify that GANs compete with and, sometimes, are superior to most state-of-the-art alternative methods. The limitations of GANs were discussed in the present study, and future research suggestions have been made to contribute to the scientific community.

Author contributions All authors contributed to the study conception and design. Material preparation, data collection, and analysis were performed by Ioannis D. Apostolopoulos, Nikolaos D. Papathanasiou, and Dimitris J. Apostolopoulos. The first draft of the manuscript was written by Ioannis D. Apostolopoulos and George S. Panayiotakis, and all authors commented on previous versions of the manuscript. All authors read and approved the final manuscript.

Funding The authors declare that no funds, grants, or other support was received during the preparation of this manuscript.

Declarations

Competing interests The authors have no relevant financial or non-financial interests to disclose.

References

1. Yinka-Banjo C, Ugot O-A. A review of generative adversarial networks and its application in cybersecurity. *Artif Intell Rev.* 2020;53:1721–36.
2. Alqahtani H, Kavakli-Thorne M, Kumar G. Applications of Generative Adversarial Networks (GANs): An Updated Review. *Arch Comput Methods Eng.* 2021;28:525–52.
3. Nensa F, Demircioglu A, Rischpler C. Artificial Intelligence in Nuclear Medicine. *J Nucl Med.* 2019;60:29S-37S.
4. Seifert R, Weber M, Kocakavuk E, Rischpler C, Kersting D. Artificial Intelligence and Machine Learning in Nuclear Medicine: Future Perspectives. *Semin Nucl Med.* 2021;51:170–7.
5. Slomka PJ, Miller RJ, Isgum I, Dey D. Application and Translation of Artificial Intelligence to Cardiovascular Imaging in Nuclear Medicine and Noncontrast CT. *Semin Nucl Med.* 2020;50:357–66.
6. Koshino K, Werner RA, Pomper MG, Bundschuh RA, Toriumi F, Higuchi T, et al. Narrative review of generative adversarial networks in medical and molecular imaging. *Ann Transl Med.* 2021;9:821–821.

7. Cheng Z, Wen J, Huang G, Yan J. Applications of artificial intelligence in nuclear medicine image generation. *Quant Imaging Med Surg.* 2021;11:2792–822.
8. Vey BL, Gichoya JW, Prater A, Hawkins CM. The Role of Generative Adversarial Networks in Radiation Reduction and Artifact Correction in Medical Imaging. *J Am Coll Radiol.* 2019;16:1273–8.
9. Arabi H, AkhavanAllaf A, Sanaat A, Shiri I, Zaidi H. The promise of artificial intelligence and deep learning in PET and SPECT imaging. *Phys Med.* 2021;83:122–37.
10. Manjooran GP, Malakkaran AJ, Joseph A, Babu HM. M S M. A Review on Cross-modality Synthesis from MRI to PET. 2021 2nd Int Conf Secure Cyber Comput Commun ICSCCC [Internet]. Jalandhar, India: IEEE; 2021. p. 126–31. Available from: <https://ieeexplore.ieee.org/document/9478170/>. Accessed 13 Oct 2021.
11. Zaharchuk G. Next generation research applications for hybrid PET/MR and PET/CT imaging using deep learning. *Eur J Nucl Med Mol Imaging.* 2019;46:2700–7.
12. Zaharchuk G, Davidzon G. Artificial Intelligence for Optimization and Interpretation of PET/CT and PET/MR Images. *Semin Nucl Med.* 2021;51:134–42.
13. Wang T, Lei Y, Fu Y, Curran WJ, Liu T, Nye JA, et al. Machine learning in quantitative PET: A review of attenuation correction and low-count image reconstruction methods. *Phys Med.* 2020;76:294–306.
14. Goodfellow I, Pouget-Abadie J, Mirza M, Xu B, Warde-Farley D, Ozair S, et al. Generative Adversarial Nets. In: Ghahramani Z, Welling M, Cortes C, Lawrence ND, Weinberger KQ, editors. *Adv Neural Inf Process Syst 27* [Internet]. Curran Associates, Inc.; 2014. p. 2672–80. Available from: <http://papers.nips.cc/paper/5423-generative-adversarial-nets.pdf>.
15. Mirza M, Osindero S. Conditional generative adversarial nets. arXiv preprint arXiv:1411.1784. 2014.
16. Isola P, Zhu J-Y, Zhou T, Efros AA. Image-to-Image Translation with Conditional Adversarial Networks. ArXiv161107004 Cs [Internet]. 2018 [cited 2021 Nov 22]; Available from: <http://arxiv.org/abs/1611.07004>.
17. Zhu J-Y, Park T, Isola P, Efros AA. Unpaired image-to-image translation using cycle-consistent adversarial networks. In: Proceedings of the IEEE international conference on computer vision. 2017. pp. 2223–2232.
18. Arjovsky M, Chintala S, Bottou L. Wasserstein generative adversarial networks. In: International conference on machine learning. PMLR; 2017. p. 214–23.
19. Apostolopoulos ID, Papathanasiou ND, Panayiotakis GS. Classification of lung nodule malignancy in computed tomography imaging utilising generative adversarial networks and semi-supervised transfer learning. *Biocybern Biomed Eng.* 2021;41:1243–57.
20. Islam J, Zhang Y. GAN-based synthetic brain PET image generation. *Brain Inform.* 2020;7:3.
21. Kimura Y, Watanabe A, Yamada T, Watanabe S, Nagaoka T, Nemoto M, et al. AI approach of cycle-consistent generative adversarial networks to synthesise PET images to train computer-aided diagnosis algorithm for dementia. *Ann Nucl Med.* 2020;34:512–5.
22. Komori S, Kimura Y, Hatano K, Kosugi T, Nishizawa S, Okada H, et al. Image-based deep-learning prediction of future FDG PET patterns in aging and dementia. *J Nucl Med.* 2019;60:1211.
23. Kim HW, Lee HE, Lee S, Oh KT, Yun M, Yoo SK. Slice-selective learning for Alzheimer’s disease classification using a generative adversarial network: a feasibility study of external validation. *Eur J Nucl Med Mol Imaging.* 2020;47:2197–206.
24. Silva G, Domingues I, Duarte H, Santos JAM. Automatic Generation of Lymphoma Post-Treatment PETs using Conditional-GANs. 2019 Digit Image Comput Tech Appl DICTA [Internet]. Perth, Australia: IEEE; 2019 [cited 2021 Nov 5]. p. 1–6. Available from: <https://ieeexplore.ieee.org/document/8945835/>.
25. Baydargil HB, Park J-S, Kang D-Y. Anomaly Analysis of Alzheimer’s Disease in PET Images Using an Unsupervised Adversarial Deep Learning Model. *Appl Sci.* 2021;11:2187.
26. Sajjad M, Ramzan F, Khan MUG, Rehman A, Kolivand M, Fati SM, et al. Deep convolutional generative adversarial network for Alzheimer’s disease classification using positron emission tomography (PET) and synthetic data augmentation. *Microsc Res Tech.* 2021. <https://doi.org/10.1002/jemt.23861>.
27. Noella RSN, Priyadarshini J. Diagnosis of Dementia Using a Generative Deep Convolution Neural Network. *Arab J Sci Eng [Internet].* 2021 [cited 2021 Nov 5]; Available from: <https://link.springer.com/https://doi.org/10.1007/s13369-021-05982-0>.
28. Amyar A, Ruan S, Vera P, Decazes P, Modzelewski R. RADIOGAN:Deep Convolutional Conditional Generative Adversarial Network to Generate PET Images. 2020 7th Int Conf Bioinforma Res Appl [Internet]. Berlin Germany: ACM; 2020 [cited 2021 Nov 3]. p. 28–33. Available from: <https://dl.acm.org/doi/https://doi.org/10.1145/3440067.3440073>.
29. Kang H, Park J-S, Cho K, Kang D-Y. Visual and Quantitative Evaluation of Amyloid Brain PET Image Synthesis with Generative Adversarial Network. *Appl Sci.* 2020;10:2628.
30. Bi L, Kim J, Kumar A, Feng D, Fulham M. Synthesis of Positron Emission Tomography (PET) Images via Multi-channel Generative Adversarial Networks (GANs). In: Cardoso MJ, Arbel T, Gao F, Kainz B, van Walsum T, Shi K, et al., editors. *Mol Imaging Reconstr Anal Mov Body Organs Stroke Imaging Treat* [Internet]. Cham: Springer International Publishing; 2017 [cited 2020 Feb 16]. p. 43–51. Available from: http://link.springer.com/https://doi.org/10.1007/978-3-319-67564-0_5.
31. Cao K, Bi L, Feng D, Kim J. Improving PET-CT Image Segmentation via Deep Multi-modality Data Augmentation. In: Deeba F, Johnson P, Würfl T, Ye JC, editors. *Mach Learn Med Image Reconstr* [Internet]. Cham: Springer International Publishing; 2020 [cited 2021 Nov 5]. p. 145–52. Available from: http://link.springer.com/https://doi.org/10.1007/978-3-030-61598-7_14.
32. Arabi H, Zeng G, Zheng G, Zaidi H. Novel adversarial semantic structure deep learning for MRI-guided attenuation correction in brain PET/MRI. *Eur J Nucl Med Mol Imaging.* 2019;46:2746–59.
33. Armanious K, Hepp T, Küstner T, Dittmann H, Nikolaou K, La Fougère C, et al. Independent attenuation correction of whole body [18F]FDG-PET using a deep learning approach with Generative Adversarial Networks. *EJNMMI Res.* 2020;10:53.
34. Hu Z, Li Y, Zou S, Xue H, Sang Z, Liu X, et al. Obtaining PET/CT images from non-attenuation corrected PET images in a single PET system using Wasserstein generative adversarial networks. *Phys Med Biol.* 2020;65:215010.
35. Jiang C, Zhang X, Zhang N, Zhang Q, Zhou C, Yuan J, et al. Synthesising PET/MR (T1-weighted) images from non-attenuation-corrected PET images. *Phys Med Biol.* 2021;66:135006.
36. Lei Y, Wang T, Dong X, Higgins K, Liu T, Curran WJ, et al. PET attenuation correction (AC) using non-AC PET-based synthetic CT. In: Bosmans H, Chen G-H, editors. *Med Imaging 2020 Phys Med Imaging* [Internet]. Houston, United States: SPIE; 2020 [cited 2021 Nov 5]. p. 154. Available from: <https://www.spiedigitallibrary.org/conference-proceedings-of-spie/11312/2548468/PET-attenuation-correction-AC-using-non-AC-PET-based-synthetic/https://doi.org/10.1117/12.2548468.full>.
37. Lei Y, Dong X, Wang T, Higgins K, Liu T, Curran WJ, et al. MRI-aided attenuation correction for PET imaging with deep learning. In: Gimi BS, Krol A, editors. *Med Imaging 2020 Biomed Appl Mol Struct Funct Imaging* [Internet]. Houston, United States: SPIE; 2020 [cited 2021 Nov 5]. p. 73. Available from: <https://www.spiedigitallibrary.org/conference-proceedings-of-spie/11317/2549388/MRI-aided-attenuation-correction-for-PET-imaging-with-deep-learning/https://doi.org/10.1117/12.2549388.full>.

38. Anaya E, Levin C. Automatic Generation of MR-based Attenuation Map using Conditional Generative Adversarial Network for Attenuation Correction in PET/MR. 2020 IEEE Nucl Sci Symp Med Imaging Conf NSSMIC [Internet]. Boston, MA, USA: IEEE; 2020 [cited 2021 Nov 5]. p. 1–3. Available from: <https://ieeexplore.ieee.org/document/9507903/>.
39. Armanious K, Küstner T, Reimold M, Nikolaou K, La Fougère C, Yang B, Gatidis S. 18 Independent brain F-FDG PET attenuation correction using a deep learning approach with Generative Adversarial Networks. *Hell J Nucl Med.* 2019;22:179–86.
40. Colmeiro RR, Verrastro C, Minsky D, Grosjes T. Whole Body Positron Emission Tomography Attenuation Correction Map Synthesizing using 3D Deep Generative Adversarial Networks [Internet]. In Review; 2020 Jul. Available from: <https://www.researchsquare.com/article/rs-46953/v1>. Accessed 05 Nov 2021.
41. Dong X, Lei Y, Wang T, Higgins K, Liu T, Curran WJ, et al. Deep learning-based attenuation correction in the absence of structural information for whole-body positron emission tomography imaging. *Phys Med Biol.* 2020;65:055011.
42. Gong K, Yang J, Larson PEZ, Behr SC, Hope TA, Seo Y, et al. MR-Based Attenuation Correction for Brain PET Using 3-D Cycle-Consistent Adversarial Network. *IEEE Trans Radiat Plasma Med Sci.* 2021;5:185–92.
43. Pozaruk A, Pawar K, Li S, Carey A, Cheng J, Sudarshan VP, et al. Augmented deep learning model for improved quantitative accuracy of MR-based PET attenuation correction in PSMA PET-MRI prostate imaging. *Eur J Nucl Med Mol Imaging.* 2021;48:9–20.
44. Qian P, Xu K, Wang T, Zheng Q, Yang H, Baydoun A, et al. Estimating CT from MR Abdominal Images Using Novel Generative Adversarial Networks. *J Grid Comput.* 2020;18:211–26.
45. Tao L, Li X, Fisher J, Levin CS. Application of Conditional Adversarial Networks for Automatic Generation of MR-based Attenuation Map in PET/MR. 2018 IEEE Nucl Sci Symp Med Imaging Conf Proc NSSMIC [Internet]. Sydney, Australia: IEEE; 2018 [cited 2021 Nov 5]. p. 1–3. Available from: <https://ieeexplore.ieee.org/document/8824444/>.
46. Tao L, Fisher J, Anaya E, Li X, Levin CS. Pseudo CT Image Synthesis and Bone Segmentation From MR Images Using Adversarial Networks With Residual Blocks for MR-Based Attenuation Correction of Brain PET Data. *IEEE Trans Radiat Plasma Med Sci.* 2021;5:193–201.
47. Li Y, Wu W. A deep learning-based approach for direct PET attenuation correction using Wasserstein generative adversarial network. *J Phys Conf Ser.* 2021;1848:012006.
48. Yang X, Lei Y, Dong X, Wang T, Higgins K, Liu T, et al. Attenuation and Scatter Correction for Whole-body PET Using 3D Generative Adversarial Networks. *J Nucl Med.* 2019;60:174.
49. Fukui R, Fujii S, Ninomiya H, Fujiwara Y, Ida T. Generation of the Pseudo CT Image Based on the Deep Learning Technique Aimed for the Attenuation Correction of the PET Image. *Jpn J Radiol Technol.* 2020;76:1152–62.
50. Schaefferkoetter J, Yan J, Moon S, Chan R, Ortega C, Metser U, et al. Deep learning for whole-body medical image generation. *Eur J Nucl Med Mol Imaging.* 2021;48:3817–26.
51. Dong X, Wang T, Lei Y, Higgins K, Liu T, Curran WJ, et al. Synthetic CT generation from non-attenuation corrected PET images for whole-body PET imaging. *Phys Med Biol.* 2019;64:215016.
52. Geng M, Meng X, Yu J, Zhu L, Jin L, Jiang Z, et al. Content-Noise Complementary Learning for Medical Image Denoising. *IEEE Trans Med Imaging.* 2021;41(2):407–19.
53. Sundar LK, Iommi D, Muzik O, Chalampalakis Z, Klebermass EM, Hienert M, et al. Conditional Generative Adversarial Networks Aided Motion Correction of Dynamic ¹⁸F-FDG PET Brain Studies. *J Nucl Med.* 2021;62:871–80.
54. Du Q, Ren X, Wang J, Qiang Y, Yang X, Kazihise NG. Iterative PET image reconstruction using cascaded data consistency generative adversarial network. *IET Image Process.* 2020;14:3989–99.
55. Shiyam Sundar L, Iommi D, Spencer B, Wang Q, Cherry S, Beyer T, et al. Data-driven motion compensation using cGAN for total-body [18F]FDG-PET imaging. *J Nucl Med.* 2021;62:35.
56. Zhou B, Tsai Y-J, Chen X, Duncan JS, Liu C. MDPET: A Unified Motion Correction and Denoising Adversarial Network for Low-Dose Gated PET. *IEEE Trans Med Imaging.* 2021;40:3154–64.
57. Wang Y, Zhou L, Yu B, Wang L, Zu C, Lalush DS, et al. 3D Auto-Context-Based Locality Adaptive Multi-Modality GANs for PET Synthesis. *IEEE Trans Med Imaging.* 2019;38:1328–39.
58. Wang Y, Yu B, Wang L, Zu C, Lalush DS, Lin W, et al. 3D conditional generative adversarial networks for high-quality PET image estimation at low dose. *Neuroimage.* 2018;174:550–62.
59. Ouyang J, Chen KT, Gong E, Pauly J, Zaharchuk G. Ultra-low-dose PET reconstruction using generative adversarial network with feature matching and task-specific perceptual loss. *Med Phys.* 2019;46:3555–64.
60. Chen KT, Gong E, de Carvalho Macruz FB, Xu J, Boumis A, Khalighi M, et al. Ultra-Low-Dose ¹⁸F-Florbetaben Amyloid PET Imaging Using Deep Learning with Multi-Contrast MRI Inputs. *Radiology.* 2019;290:649–56.
61. Hu Z, Xue H, Zhang Q, Gao J, Zhang N, Zou S, et al. DPIP-Net: Direct PET Image Reconstruction Based on the Wasserstein Generative Adversarial Network. *IEEE Trans Radiat Plasma Med Sci.* 2021;5:35–43.
62. Sanaat A, Shiri I, Arabi H, Mainta I, Nkoulou R, Zaidi H. Whole-body PET Image Synthesis from Low-Dose Images Using Cycle-consistent Generative Adversarial Networks. 2020 IEEE Nucl Sci Symp Med Imaging Conf NSSMIC [Internet]. Boston, MA, USA: IEEE; 2020 [cited 2021 Nov 5]. p. 1–3. Available from: <https://ieeexplore.ieee.org/document/9507947/>.
63. Xue H, Zhang Q, Zou S, Zhang W, Zhou C, Tie C, et al. LCP-Net: low-count PET image reconstruction using the domain transform and cycle-consistent generative adversarial networks. *Quant Imaging Med Surg.* 2021;11:749–62.
64. Du Q, Qiang Y, Yang W, Wang Y, Ma Y, Zia MB. DRGAN: a deep residual generative adversarial network for PET image reconstruction. *IET Image Process.* 2020;14:1690–700.
65. Lei Y, Wang T, Dong X, Higgins K, Liu T, Curran WJ, et al. Low dose PET imaging with CT-aided cycle-consistent adversarial networks. In: Bosmans H, Chen G-H, editors. *Med Imaging 2020 Phys Med Imaging* [Internet]. Houston, United States: SPIE; 2020 [cited 2021 Nov 5]. p. 152. Available from: <https://www.spiedigitallibrary.org/conference-proceedings-of-spie/11312/2549386/Low-dose-PET-imaging-with-CT-aided-cycle-consistent-adversarial><https://doi.org/10.1117/12.2549386.full>.
66. Lei Y, Dong X, Wang T, Higgins K, Liu T, Curran WJ, et al. Estimating standard-dose PET from low-dose PET with deep learning. In: Landman BA, Išgum I, editors. *Med Imaging 2020 Image Process* [Internet]. Houston, United States: SPIE; 2020 [cited 2021 Nov 5]. p. 73. Available from: <https://www.spiedigitallibrary.org/conference-proceedings-of-spie/11313/2548461/Estimating-standard-dose-PET-from-low-dose-PET-with-deep><https://doi.org/10.1117/12.2548461.full>.
67. Zhao K, Zhou L, Gao S, Wang X, Wang Y, Zhao X, et al. Study of low-dose PET image recovery using supervised learning with CycleGAN. Hatt M, editor. *PLOS ONE.* 2020; 15:e0238455.
68. Gong Y, Shan H, Teng Y, Tu N, Li M, Liang G, et al. Parameter-Transferred Wasserstein Generative Adversarial Network (PT-WGAN) for Low-Dose PET Image Denoising. *IEEE Trans Radiat Plasma Med Sci.* 2021;5:213–23.

69. Lu W, Onofrey JA, Lu Y, Shi L, Ma T, Liu Y, et al. An investigation of quantitative accuracy for deep learning based de-noising in oncological PET. *Phys Med Biol*. 2019;64:165019.
70. Wang Y, Zhou L, Wang L, Yu B, Zu C, Lalush DS, et al. Locality Adaptive Multi-modality GANs for High-Quality PET Image Synthesis. In: Frangi AF, Schnabel JA, Davatzikos C, Alberola-López C, Fichtinger G, editors. *Med Image Comput Comput Assist Interv – MICCAI 2018* [Internet]. Cham: Springer International Publishing; 2018 [cited 2021 Nov 5]. p. 329–37. Available from: http://link.springer.com/https://doi.org/10.1007/978-3-030-00928-1_38.
71. Xie Z, Baikejiang R, Li T, Zhang X, Gong K, Zhang M, et al. Generative adversarial network based regularised image reconstruction for PET. *Phys Med Biol*. 2020;65:125016.
72. Zhou L, Schaefferkoetter JD, Tham IWK, Huang G, Yan J. Supervised learning with cyclegan for low-dose FDG PET image de-noising. *Med Image Anal*. 2020;65:101770.
73. Sanaat A, Shiri I, Arabi H, Mainta I, Nkoulou R, Zaidi H. Deep learning-assisted ultra-fast/low-dose whole-body PET/CT imaging. *Eur J Nucl Med Mol Imaging*. 2021;48:2405–15.
74. Jeong YJ, Park HS, Jeong JE, Yoon HJ, Jeon K, Cho K, et al. Restoration of amyloid PET images obtained with short-time data using a generative adversarial networks framework. *Sci Rep*. 2021;11:4825.
75. Sanaat A, Mirsadeghi E, Razeghi B, Ginovart N, Zaidi H. Fast Dynamic Brain PET Imaging Using a Generative Adversarial Network. 2020 IEEE Nucl Sci Symp Med Imaging Conf NSSMIC [Internet]. Boston, MA, USA: IEEE; 2020 [cited 2021 Nov 5]. p. 1–3. Available from: <https://ieeexplore.ieee.org/document/9507894/>.
76. Kim J-W, Kim J-Y, Lim H, Kim J. Comparative Evaluation of 18 F-FDG Brain PET/CT AI Images Obtained Using Generative Adversarial Network. *Korean J Nucl Med Technol. The Korean Society of Nuclear Medicine Technology*. 2020; 24:15–9.
77. Xue H, Teng Y, Tie C, Wan Q, Wu J, Li M, et al. A 3D attention residual encoder–decoder least-square GAN for low-count PET de-noising. *Nucl Instrum Methods Phys Res Sect Accel Spectrometers Detect Assoc Equip*. 2020;983:164638.
78. Lei Y, Dong X, Wang T, Higgins K, Liu T, Curran WJ, et al. Whole-body PET estimation from low count statistics using cycle-consistent generative adversarial networks. *Phys Med Biol*. 2019;64:215017.
79. Liu Z, Chen H, Liu H. Deep Learning Based Framework for Direct Reconstruction of PET Images. In: Shen D, Liu T, Peters TM, Staib LH, Essert C, Zhou S, et al., editors. *Med Image Comput Comput Assist Interv – MICCAI 2019* [Internet]. Cham: Springer International Publishing; 2019 [cited 2021 Nov 5]. p. 48–56. Available from: http://link.springer.com/https://doi.org/10.1007/978-3-030-32248-9_6.
80. Song T-A, Chowdhury SR, Yang F, Dutta J. PET image super-resolution using generative adversarial networks. *Neural Netw*. 2020;125:83–91.
81. Song T-A, Roy Chowdhury S, Yang F, Dutta J. Self Supervised Super-Resolution PET Using A Generative Adversarial Network. 2019 IEEE Nucl Sci Symp Med Imaging Conf NSSMIC [Internet]. Manchester, United Kingdom: IEEE; 2019 [cited 2021 Nov 5]. p. 1–3. Available from: <https://ieeexplore.ieee.org/document/9059947/>.
82. Oh KT, Kim D, Ye BS, Lee S, Yun M, Yoo SK. Segmentation of white matter hyperintensities on 18F-FDG PET/CT images with a generative adversarial network. *Eur J Nucl Med Mol Imaging*. 2021;48:3422–31.
83. Oh KT, Lee S, Lee H, Yun M, Yoo SK. Semantic Segmentation of White Matter in FDG-PET Using Generative Adversarial Network. *J Digit Imaging*. 2020;33:816–25.
84. Wu X, Bi L, Fulham M, Kim J. Unsupervised Positron Emission Tomography Tumor Segmentation via GAN based Adversarial Auto-Encoder. 2020 16th Int Conf Control Autom Robot Vis ICARCV [Internet]. Shenzhen, China: IEEE; 2020 [cited 2021 Nov 5]. p. 448–53. Available from: <https://ieeexplore.ieee.org/document/9305364/>.
85. Yousefirizi F, Rahmim A. GAN-Based Bi-Modal Segmentation Using Mumford-Shah Loss: Application to Head and Neck Tumors in PET-CT Images. In: Andrearczyk V, Oreiller V, Depoeringe A, editors. *Head Neck Tumor Segmentation* [Internet]. Cham: Springer International Publishing; 2021 [cited 2021 Nov 5]. p. 99–108. Available from: http://link.springer.com/https://doi.org/10.1007/978-3-030-67194-5_11.
86. Ma J, Xu H, Jiang J, Mei X, Zhang X-P. DDcGAN: A Dual-Discriminator Conditional Generative Adversarial Network for Multi-Resolution Image Fusion. *IEEE Trans Image Process*. 2020;29:4980–95.
87. Kang J, Lu W, Zhang W. Fusion of Brain PET and MRI Images Using Tissue-Aware Conditional Generative Adversarial Network With Joint Loss. *IEEE Access*. 2020;8:6368–78.
88. Huang J, Le Z, Ma Y, Fan F, Zhang H, Yang L. MGMDcGAN: Medical Image Fusion Using Multi-Generator Multi-Discriminator Conditional Generative Adversarial Network. *IEEE Access*. 2020;8:55145–57.
89. Yang Z, Chen Y, Le Z, Fan F, Pan E. Multi-Source Medical Image Fusion Based on Wasserstein Generative Adversarial Networks. *IEEE Access*. 2019;7:175947–58.
90. Liu H, Nai Y-H, Saridin F, Tanaka T, O’Doherty J, Hilal S, et al. Improved amyloid burden quantification with non-specific estimates using deep learning. *Eur J Nucl Med Mol Imaging*. 2021;48:1842–53.
91. Kang SK, Choi H, Lee JS. Translating amyloid PET of different radiotracers by a deep generative model for interchangeability. *NeuroImage*. 2021;232:117890.
92. Kang SK, Seo S, Shin SA, Byun MS, Lee DY, Kim YK, et al. Adaptive template generation for amyloid PET using a deep learning approach. *Hum Brain Mapp*. 2018;39:3769–78.
93. Liu H, Nai Y-H, Chen C, Reilhac A. Deep Learning-Based Estimation of Non-Specific Uptake in Amyloid-PET Images from Structural MRI for Improved Quantification of Amyloid Load in Alzheimer’s Disease. 2020 IEEE 33rd Int Symp Comput-Based Med Syst CBMS [Internet]. Rochester, MN, USA: IEEE; 2020 [cited 2021 Nov 5]. p. 573–8. Available from: <https://ieeexplore.ieee.org/document/9182970/>.
94. Ma S, Hu Z, Ye K, Zhang X, Wang Y, Peng H. Feasibility study of patient-specific dose verification in proton therapy utilising positron emission tomography (PET) and generative adversarial network (GAN). *Med Phys*. 2020;47:5194–208.
95. Hognon C, Tixier F, Colin T, Gallinato O, Visvikis D, Jaouen V. Influence of gradient difference loss on MR to PET brain image synthesis using GANs. *J Nucl Med*. 2020;61:1431.
96. Hu S, Lei B, Wang S, Wang Y, Feng Z, Shen Y. Bidirectional Mapping Generative Adversarial Networks for Brain MR to PET Synthesis. *IEEE Trans Med Imaging*. 2022;41(1):145–57.
97. Wei W, Poirion E, Bodini B, Durrleman S, Ayache N, Stankoff B, et al. Predicting PET-derived demyelination from multi-modal MRI using sketcher-refiner adversarial training for multiple sclerosis. *Med Image Anal*. 2019;58:101546.
98. Pan Y, Liu M, Lian C, Xia Y, Shen D. Spatially-Constrained Fisher Representation for Brain Disease Identification With Incomplete Multi-Modal Neuroimages. *IEEE Trans Med Imaging*. 2020;39:2965–75.
99. Shin H-C, Ihsani A, Mandava S, Sreenivas ST, Forster C, Cha J et al. GANBERT: Generative Adversarial Networks with Bidirectional Encoder Representations from Transformers for MRI to PET synthesis. *ArXiv200804393 Cs Eess* [Internet]. 2020 [cited 2021 Nov 5]; Available from: <http://arxiv.org/abs/2008.04393>.

100. Hu S, Yuan J, Wang S. Cross-modality Synthesis from MRI to PET Using Adversarial U-Net with Different Normalisation. 2019 Int Conf Med Imaging Phys Eng ICMPE [Internet]. Shenzhen, China: IEEE; 2019 [cited 2021 Nov 5]. p. 1–5. Available from: <https://ieeexplore.ieee.org/document/9098219>.
101. Hu S, Shen Y, Wang S, Lei B. Brain MR to PET Synthesis via Bidirectional Generative Adversarial Network. In: Martel AL, Abolmaesumi P, Stoyanov D, Mateus D, Zuluaga MA, Zhou SK, et al., editors. Med Image Comput Assist Interv – MICCAI 2020 [Internet]. Cham: Springer International Publishing; 2020 [cited 2021 Nov 5]. p. 698–707. Available from: https://link.springer.com/https://doi.org/10.1007/978-3-030-59713-9_67.
102. Jung MM, van den Berg B, Postma E, Huijbers W. Inferring PET from MRI with pix2pix. Inferring PET MRI Pix2pix [Internet]. 2018. Available from: <https://bnaic2018.nl/>.
103. Lin W, Lin W, Chen G, Zhang H, Gao Q, Huang Y, et al. Bidirectional Mapping of Brain MRI and PET With 3D Reversible GAN for the Diagnosis of Alzheimer's Disease. Front Neurosci. 2021;15:646013.
104. Lan H, the Alzheimer Disease Neuroimaging Initiative, Toga AW, Sepelrband F. Three-dimensional self-attention conditional GAN with spectral normalisation for multi-modal neuroimaging synthesis. Magn Reson Med. 2021;86:1718–33.
105. Yaakub SN, McGinnity CJ, Clough JR, Kerfoot E, Girard N, Guedj E et al. Pseudo-normal PET Synthesis with Generative Adversarial Networks for Localising Hypometabolism in Epilepsies. In: Burgos N, Gooya A, Svoboda D, editors. Simul Synth Med Imaging [Internet]. Cham: Springer International Publishing; 2019 [cited 2021 Nov 5]. p. 42–51. Available from: http://link.springer.com/https://doi.org/10.1007/978-3-030-32778-1_5.
106. Pan Y, Liu M, Lian C, Zhou T, Xia Y, Shen D. Synthesizing Missing PET from MRI with Cycle-consistent Generative Adversarial Networks for Alzheimer's Disease Diagnosis. In: Frangi AF, Schnabel JA, Davatzikos C, Alberola-López C, Fichtinger G, editors. Med Image Comput Assist Interv – MICCAI 2018 [Internet]. Cham: Springer International Publishing; 2018 [cited 2021 Nov 5]. p. 455–63. Available from: http://link.springer.com/https://doi.org/10.1007/978-3-030-00931-1_52.
107. Sikka A, Skand, Virk JS, Bathula DR. MRI to PET Cross-Modality Translation using Globally and Locally Aware GAN (GLA-GAN) for Multi-Modal Diagnosis of Alzheimer's Disease. ArXiv210802160 Cs Eess [Internet]. 2021 [cited 2021 Nov 5]; Available from: <http://arxiv.org/abs/2108.02160>.
108. Yan Y, Lee H, Somer E, Grau V. Generation of Amyloid PET Images via Conditional Adversarial Training for Predicting Progression to Alzheimer's Disease. In: Rekik I, Unal G, Adeli E, Park SH, editors. Predict Intell Med [Internet]. Cham: Springer International Publishing; 2018 [cited 2021 Nov 5]. p. 26–33. Available from: http://link.springer.com/https://doi.org/10.1007/978-3-030-00320-3_4.
109. Gao X, Shi F, Shen D, Liu M. Task-induced Pyramid and Attention GAN for Multi-modal Brain Image Imputation and Classification in Alzheimers disease. IEEE J Biomed Health Inform. 2021;26(1):36–43.
110. Choi H, Lee DS. Generation of Structural MR Images from Amyloid PET: Application to MR-Less Quantification. J Nucl Med. 2018;59:1111–7.
111. Armanious K, Jiang C, Fischer M, Küstner T, Hepp T, Nikolaou K, et al. MedGAN: Medical image translation using GANs. Comput Med Imaging Graph. 2020;79:101684.
112. Santini G, Fourcade C, Moreau N, Rousseau C, Ferrer L, Lacombe M et al. Unpaired PET/CT image synthesis of liver region using CycleGAN. In: Brieva J, Lepore N, Romero Castro E, Linguraru MG, editors. 16th Int Symp Med Inf Process Anal [Internet]. Lima, Peru: SPIE; 2020 [cited 2021 Nov 5]. p. 6. Available from: <https://www.spiedigitallibrary.org/conference-proceedings-of-spie/11583/2576095/Unpaired-PETCT-image-synthesis-of-liver-region-using-CycleGAN/https://doi.org/10.1117/12.2576095.full>.
113. Sharma A, Jindal N. Cross-Modality Breast Image Translation with Improved Resolution Using Generative Adversarial Networks. Wirel Pers Commun. 2021;119:2877–91.
114. Ben-Cohen A, Klang E, Raskin SP, Soffer S, Ben-Haim S, Konen E, et al. Cross-modality synthesis from CT to PET using FCN and GAN networks for improved automated lesion detection. Eng Appl Artif Intell. 2019;78:186–94.
115. Leydon P, O'Connell M, Greene D, Curran K. Synthetic positron emission tomography using conditional-generative adversarial networks for healthy bone marrow baseline image generation. IMVIP 2019: Irish Machine Vision & Image Processing, Technological University Dublin: Dublin, Ireland; 2019. <https://doi.org/10.21427/xmkn-d265>.
116. Liebgott A, Hindere D, Armanious K, Bartler A, Nikolaou K, Gatidis S et al. Prediction of FDG uptake in Lung Tumors from CT Images Using Generative Adversarial Networks. 2019. pp. 1–5. <https://doi.org/10.23919/EUSIPCO.2019.8902935>.
117. Ben-Cohen A, Klang E, Raskin SP, Amitai MM, Greenspan H. Virtual PET Images from CT Data Using Deep Convolutional Networks: Initial Results. In: Tsafaris SA, Gooya A, Frangi AF, Prince JL, editors. Simul Synth Med Imaging [Internet]. Cham: Springer International Publishing; 2017 [cited 2021 Nov 5]. p. 49–57. Available from: http://link.springer.com/https://doi.org/10.1007/978-3-319-68127-6_6.
118. Huang B, Chen Z, Law M, Feng S, Li Q, Huang B. Progressive Generative Adversarial Networks: Deep Learning in Head and Neck Cancer CT Images to Synthesized PET Images Generation for Hybrid PET/CT Application. DEStech Trans Comput Sci Eng [Internet]. 2018 [cited 2021 Nov 5]; Available from: <http://dpi-proceedings.com/index.php/dtcsev/article/view/24701>.
119. Plachouris D, Tzolas I, Gatos I, Papadimitroulas P, Spyridonidis T, Apostolopoulos D, et al. A deep-learning-based prediction model for the biodistribution of ⁹⁰Y microspheres in liver radioembolisation. Med Phys. 2021;48:7427–38.
120. Chen JS, Coyner AS, Chan RVP, Hartnett ME, Moshfeghi DM, Owen LA, et al. Deepfakes in Ophthalmology. Ophthalmol Sci. 2021;1:100079.
121. Chu LC, Anandkumar A, Shin HC, Fishman EK. The Potential Dangers of Artificial Intelligence for Radiology and Radiologists. J Am Coll Radiol. 2020;17:1309–11.
122. Apostolopoulos ID, Pintelas EG, Livieris IE, Apostolopoulos DJ, Papathanasiou ND, Pintelas PE, et al. Automatic classification of solitary pulmonary nodules in PET/CT imaging employing transfer learning techniques. Med Biol Eng Comput. 2021;59:1299–310.
123. Apostolopoulos ID, Apostolopoulos DI, Spyridonidis TI, Papathanasiou ND, Panayiotakis GS. Multi-input deep learning approach for Cardiovascular Disease diagnosis using Myocardial Perfusion Imaging and clinical data. Phys Med. 2021;84:168–77.

Publisher's note Springer Nature remains neutral with regard to jurisdictional claims in published maps and institutional affiliations.